OPEN

MondoA and AKI and AKI-to-CKD Transition

Shihomi Maeda,[1] Shinsuke Sakai,[1] Yoshitsugu Takabatake,[1] Takeshi Yamamoto,[1] Satoshi Minami,[1] Jun Nakamura,[1] Tomoko Namba-Hamano,[1] Atsushi Takahashi,[1] Jun Matsuda,[1] Hiroaki Yonishi,[1] Sho Matsui,[1] Atsuhiro Imai,[1] Ryuya Edahiro,[2,3] Hitomi Yamamoto-Imoto,[4] Isao Matsui,[1] Seiji Takashima,[5] Ryoichi Imamura,[6] Norio Nonomura,[7] Motoko Yanagita,[8,9] Yukinori Okada,[2,10,11,12,13] Andrea Ballabio,[14,15,16,17] Shuhei Nakamura,[18] Tamotsu Yoshimori,[4,19,20] and Yoshitaka Isaka[1]

Key Points

- The expression of MondoA was decreased in the renal tubules of patients with CKD.
- Genetic ablation of MondoA in proximal tubules inhibited autophagy and increased vulnerability to AKI through increased expression of Rubicon.
- MondoA ablation during the recovery phase after ischemia-reperfusion aggravated kidney injury through downregulation of the transcription factor EB-peroxisome proliferator-activated receptor-γ coactivator-1α axis.

Abstract

Background Elderly individuals and patients with CKD are at a higher risk of AKI. The transcription factor MondoA is downregulated in the kidneys of aged individuals or patients with AKI; however, its roles in AKI development and the AKI-to-CKD transition remain unknown.

Methods We investigated the expression of MondoA in human kidney biopsy samples, ischemia-reperfusion–injured (IRI) mouse kidneys, and cultured proximal tubular epithelial cells under hypoxia/reoxygenation. The role of MondoA during the initial and recovery phases after IRI was evaluated using proximal tubule–specific *MondoA* knockout mice and *MondoA*-deficient proximal tubular epithelial cells. Furthermore, we explored the involvement of Rubicon and transcription factor EB (TFEB), both of which are downstream factors of MondoA.

Results MONDOA expression was decreased in the renal tubules of patients with CKD. In mouse kidneys, MondoA expression was decreased under ischemia, whereas its expression was increased during reperfusion. Genetic ablation of *MondoA* in proximal tubular epithelial cells inhibited autophagy and increased vulnerability to AKI through increased expression of Rubicon. Ablation of *Rubicon* in *MondoA*-deficient IRI kidneys activated autophagy and protected mitochondrial function. *MondoA* ablation during the recovery phase after ischemia-reperfusion aggravated kidney injury through downregulation of the TFEB-peroxisome proliferator-activated receptor-γ coactivator-1α axis. Pharmacological upregulation of TFEB contributed to maintaining mitochondrial biogenesis and increased peroxisome proliferator-activated receptor-γ coactivator-1α transcription.

Conclusions Our findings demonstrate that MondoA protected against vulnerability to AKI by maintaining autophagy and subsequently supporting mitochondrial function to prevent progression to CKD.

JASN 00: 1–19, 2024. doi: https://doi.org/10.1681/ASN.0000000000000414

Introduction

AKI is a high-risk condition associated with elevated mortality and mobility rates and high hospitalization costs.[1,2] Although previously thought to be reversible, AKI is now widely known to be an important risk factor for the development of CKD and kidney failure,[3,4] thus giving rise to the concept of the AKI-to-CKD transition. The risk of CKD progression after AKI is influenced by the severity and duration of AKI and patient characteristics in the acute phase. Epidemiological studies have demonstrated that

Due to the number of contributing authors, the affiliations are listed at the end of this article.

Correspondence: Dr. Takeshi Yamamoto, email: tyamamoto@kid.med.osaka-u.ac.jp

Received: October 31, 2023 **Accepted:** May 24, 2024
Published Online Ahead of Print: May 31, 2024

S.M. and S.S. contributed equally to this work.

elderly individuals and those with preexisting CKD are more vulnerable to AKI and exhibit a higher incidence of severe CKD (AKI on CKD).[3,5,6] This susceptibility can be attributed to both reduced renal reserve due to age-related morphologic and functional changes and exposure to a variety of nephrotoxic drugs for the management of preexisting disease. The precise cellular and molecular mechanisms underlying the AKI-to-CKD transition and disease progression in patients with CKD are largely unknown. However, there is no doubt that vulnerability to AKI is exacerbated in these populations.

Our previous research highlighted the significance of macroautophagy/autophagy of proximal tubular epithelial cells in terms of reducing the vulnerability to AKI.[7–9] In addition, autophagy plays a key role in counteracting the progression of chronic pathological conditions, including kidney aging[10] and metabolic syndrome–related diseases.[11–13] However, autophagy is dysregulated during aging, obesity, and diabetes, which promotes kidney disease progression, partly through mitochondrial dysfunction.[10,14] Thus, to prevent disease progression in patients with CKD, it is critically important to elucidate the mechanisms behind their vulnerability to AKI.

Recent findings indicate that MLX interacting protein (MLXIP), which encodes MondoA, delays cellular senescence, at least in part, by activating autophagy through suppression of run domain beclin-1–interacting and cysteine-rich domain-containing protein (RUBCN)/Rubicon, a negative regulator of autophagosome maturation.[15] Decreased MONDOA expression is correlated with human kidney aging and ischemic AKI.[15,16] MondoA and its obligate transcription partner Mlx are basic helix-loop-helix leucine zipper transcription factors that sense and execute a glucose-responsive transcriptional program.[17,18] Intriguingly, studies in *Caenorhabditis elegans* have unveiled a Myc-like helix-loop-helix transcription factor network, comprising the Mondo/Max-like complex (MML-1/MXL-2), that is required for longevity induced by germline removal.[19] Moreover, by downregulating mechanistic target of rapamycin (mTOR) signaling, MML-1/MondoA regulates the nuclear localization and activity of helix-loop-helix-30/transcription factor EB (TFEB), a convergent regulator of autophagy, lysosome biogenesis, and longevity.[19,20] Nevertheless, research on MondoA has predominantly focused on cultured cells, particularly malignant cells, leaving the precise role of MondoA in kidney disease progression largely unexplored.

In this study, we hypothesized that diminished MONDOA expression in the kidneys of patients with CKD would heighten their vulnerability to AKI, impairing recovery and expediting the AKI-to-CKD transition. Therefore, we first analyzed MONDOA expression in the kidneys of patients with CKD. We then investigated the dynamics of MondoA expression, its transcription activity, and its roles in proximal tubular epithelial cells during both AKI and the AKI-to-CKD transition, with a focus on Rubicon and TFEB.

Methods

Cell Culture

Isolation and immortalization of proximal tubular epithelial cells was performed as previously described with some modifications.[7] In brief, *MondoA*-floxed proximal tubular epithelial cells were isolated from 3-week-old mice and immortalized by using pEF321-T, an SV-40 large T antigen expression vector. Cells derived from a single colony were transfected with the pCAG-Cre vector (Addgene, 13775) to construct *MondoA*-deficient proximal tubular epithelial cell lines by using Lipofectamine3000 (Thermo Fisher, Courtaboeuf, France), followed by puromycin selection. We used Cre-negative *MondoA*-floxed proximal tubular epithelial cells as a control. *Rubicon*-deficient proximal tubular epithelial cells were isolated and immortalized as described previously.[21,22] *MondoA* knockdown in *Rubicon*-deficient proximal tubular epithelial cells was conducted as described previously using MISSION short hairpin RNA Lentiviral Transduction Particles (Sigma-Aldrich, Saint Louis, MO, TRCN0000124922) with puromycin (Wisent, QC, Canada, 450-162-XL) selection.[23] Briefly, virus-containing supernatants were added to proximal tubular epithelial cells in permissive conditions for 16 hours. Puromycin was added 48 hours later, and puromycin-resistant cells were pooled for further experiments. Proximal tubular epithelial cells at passage 3–10 were used in all the experiments. Proximal tubular epithelial cells were cultured in low-glucose DMEM (Nacalai Tesque, Kyoto, Japan, 08456-65) with 5% FBS (Sigma-Aldrich, F7524) at 37°C under a humidified atmosphere of 5% CO_2 and 95% air. To confirm the deficiency of MondoA, proximal tubular epithelial cells were treated with 10 mM of 2-deoxy-D-glucose (2DG, Sigma-Aldrich, D8375) for 2 hours. To assess autophagic activity, proximal tubular epithelial cells were treated with 200 nM of bafilomycin A_1 (Cayman Chemical, Ann Arbor, MI, 11038) for 1 hour at 37°C before harvest. In hypoxia/reoxygenation (H/R) experiment, proximal tubular epithelial cells were supplemented with fresh low-glucose DMEM with 5% FBS, followed by transferring to a hypoxic incubator (PHC, Tokyo, Japan, MCO-5MUV-PJ) under an atmosphere with 1% O_2, 5% CO_2, and 94% N_2 for 6 hours. Then, they were transferred back to the normoxic incubator under an atmosphere with 21% O_2. After reoxygenation for 3 hours, the cells were collected. Cells cultured in DMEM medium supplemented with 5% FBS without H/R were collected as the control samples. To enhance TFEB nuclear translocation, proximal tubular epithelial cells were treated with 50 mM of trehalose (Sigma-Aldrich, T0167). To investigate the effect of peroxisome proliferator-activated receptor-γ coactivator-1α (PGC1α) activation, proximal tubular epithelial cells were treated with 20 μM of ZLN005 (MedChemExpress, Monmouth Junction, NJ, HY-17538).

Analysis of Murine Mlxip and Downstream Factor Gene Expression in Single-Cell RNA Sequencing Dataset

Mlxip and downstream factor gene expression was analyzed with the published single-cell RNA sequencing dataset for mouse kidneys with ischemic reperfusion injury (GSE180420)[24] on R package Seurat (v4.1.0). Proximal tubular cells (S1 and S3) in kidneys of control, short ischemia-reperfusion injury (IRI) (23 minutes), and long IRI (30 minutes) samples were extracted and reanalyzed to visualize change in the *Mlxip*, *Txnip*, arrestin domain containing 4 (*Arrdc4*), *Rubcn*, *Tfeb*, and *Ppargc1a* expression pattern along with time course for each subtype after

ischemic reperfusion injury. The dot plot was produced using DotPlot() function. We performed differential expression analysis of *Mlxip* between short IRI and long IRI in the S1 and S3 segments across time course using FindMarkers() function with parameter test.use=wilcox.

Mice

Green fluorescent protein-microtubule–associated protein 1 light chain 3 (GFP-MAP1LC3) transgenic mice, *MondoA*$^{F/F}$; kidney androgen-regulated protein-Cre (KAP) mice, *Rubicon* $^{F/F}$; KAP mice and *Tfeb*$^{F/F}$; and *N*-myc downstream-regulated gene 1 (NDRG1)-Cre^{ERT2} mice on a C57BL/6N background have been described previously.[7,13,15,21,25] Proximal tubule–specific *MondoA*-deficient and *Rubicon*-deficient mice were generated by crossing mice bearing a *MondoA* flox allele with *Rubicon*$^{F/F}$; KAP mice. Tamoxifen-inducible proximal tubule–specific *MondoA*-deficient mice (*MondoA*$^{F/F}$; NDRG1) were generated by crossing mice bearing a *MondoA* flox allele with NDRG1-Cre^{ERT2} mice.[26] Only male mice were used in this study. Mice were housed in box cages, maintained on a 12-hour light/12-hour dark cycle, and fed a chow diet (Oriental Yeast, Osaka, Japan) *ad libitum*. To induce *MondoA* deletion in *MondoA*$^{F/F}$; NDRG1 mice, tamoxifen (Sigma-Aldrich, T5648; 0.1 mg/g body weight) dissolved in corn oil (Sigma-Aldrich, C8267) was injected at a concentration of 10 mg/ml 24 and 96 hours after IR operation. To investigate the effect of TFEB/PGC1α activation, vehicle, trehalose (Sigma-Aldrich, T9531; dissolved in saline, 2 mg/g body weight, 3 days a week) or ZLN005 (MedChemExpress, HY-17538; dissolved in 5% DMSO, 5% Tween 80, and 2.5% polyethylene glycol 400 in saline, 12 mg/g body weight, 3 days a week) was intraperitoneally administered 48 hours after IR. In an experiment assessing autophagic flux *in vivo*, chloroquine (CQ) (Sigma-Aldrich, C6628; 50 mg/g body weight) was injected intraperitoneally 6 hours before euthanasia.

Kidney IRI

Procedure of kidney IR and assessment of tubular injury were described previously.[7,27] Experiments were performed on 8- to 10-week-old male mice using littermate controls by an operator blinded to genotype. In brief, the animals were intraperitoneally anesthetized with butorphanol (5 mg/kg), midazolam (4 mg/kg), and medetomidine (0.5 mg/kg) and were kept on a homeothermic table. For unilateral or bilateral kidney IRI, left or both pedicles were clamped for 35 minutes, respectively. The clamps were released for reperfusion for the indicated times. Control animals were subjected to sham operation without renal pedicle clamping.

Antibodies

We used the following antibodies: antibodies for MondoA/MLXIP (Bethyl Laboratories, Montgomery, TX, A303-195A), thioredoxin interacting protein (Cell Signaling Technology, Beverly, MA, 14715), RUBCN (Cell Signaling Technology, 8465 for mouse samples; Medical and Biologic Laboratory, Nagoya, Japan, PD027 for human samples), PGC1α (Novus Biologicals, Centennial, CO, NBP1-04676), LRP2 (LDL receptor related protein 2)/MEGALIN (a gift from Dr. Michigami, Department of Bone and Mineral Research, Osaka Medical Center and Research Institute for Maternal and Child Health, Japan), TFEB (Bethyl, A303-673A for mouse samples; Cell Signaling Technology, 37785 for human samples), Lamin A/C (Cell Signaling Technology, 2032), glyceraldehyde-3-phosphate dehydrogenase (GeneTex, Irvine, CA, GTX100118), S6 ribosomal protein (Cell Signaling Technology, 2217), phospho-S6 ribosomal protein (Ser235/236; Cell Signaling Technology, 2211), actin beta (Sigma-Aldrich, A5316), lysosomal-associated membrane protein 1 (LAMP1) (BD Biosciences, Franklin Lakes, NJ, 553792), MAP1LC3B (for western blotting; Cell Signaling Technology, 2775; for immunostaining; Medical and Biologic Laboratory, PM036), COL1A1 (Abcam, Cambridge, United Kingdom, ab34710), sequestosome 1 (SQSTM1)/p62 (Medical and Biological Laboratory, PM045), PRDX3 (peroxiredoxin 3 [Prdx3]) (Abcam, Ab73349), vascular cell adhesion molecule 1 (VCAM1) (Abcam, Ab134047), biotinylated secondary antibodies (Vector Laboratories, BA-1000, BA-2001, BA-4000, and BA-7000) (Vector Laboratories, Burlingame, CA), horseradish peroxidase–conjugated secondary antibodies (DAKO, P0447, P0448, P0449, and P0450) (DAKO, Glostrup, Denmark), and Alexa-conjugated secondary antibodies (Thermo Fisher Scientific, A21206, A21208, A21434, and A31572) (Invitrogen, Carlsbad, CA).

Histological Analysis

Histological analysis was performed as described previously with modifications.[10] The following were also performed as described previously: fluorescence and immunofluorescence microscopy analysis *in vitro*,[28] electron microscopy analysis, succinate dehydrogenase (SDH) staining on fresh frozen sections,[29] Masson-trichrome staining,[30] terminal deoxynucleotidyl transferase–mediated digoxigenin-deoxy uridine nick-end labeling staining, counting of GFP-MAP1LC3 dots, and assessment of kidney injury.[10,11,27] Immunohistochemical staining was performed on the paraffin-embedded sections. After deparaffinization and rehydration, antigen retrieval was performed by autoclaving in 0.01 mM citrate buffer (pH 6.0)[8] or Tris-EDTA buffer (10 mM Tris, 1 mM EDTA, pH 9.0) for 10 minutes at 120°C. In particular, the Tris-EDTA buffer was effective for achieving clear RUBCN staining in human samples.[31] For immunofluorescence study for LC3 and LAMP1, the colocalization of LAMP1-positive dots and MAP1LC3-positive dots was calculated using National Institutes of Health ImageJ imaging software. Autophagosomes were identified as ribosome-free double-membrane or partially double–membrane vesicles with identified cargo or contents of comparable density with the surrounding cytosol; autolysosomes were identified as single-membrane vesicles with contents at a density lower than the surrounding cytosol and cargo suggestive of degradation. For SDH staining, Masson-trichrome staining, and COL1A1 staining, 5–10 nonoverlapping high-power (×400) fields in the cortex area of each kidney section were captured and quantified using National Institutes of Health ImageJ imaging software. The positively stained area was expressed as a percentage of the total area. In all quantitative or semiquantitative analysis of histological staining, at least ten

high-power fields in each kidney were reviewed by three nephrologists (S. Maeda, S. Sakai, and T. Yamamoto) in a blinded manner.

Nuclear and Cytosolic/Cytoplasmic Fractionation

Kidney nuclear and cytosolic fractionation was performed as described previously.[25,32]

Assessment of TFEB Nuclear Localization *In Vitro*

TFEB was translocated to the nucleus only when nuclear TFEB was clearly detected. The percentage of proximal tubular epithelial cells exhibiting TFEB nuclear translocation was determined by counting more than 100 cells from more than ten fields.[33]

Assessment of Mitochondrial Function and Biogenesis

To measure mitochondrial membrane potential or reactive oxygen species (ROS) production, proximal tubular epithelial cells were cultured on 35-mm glass-bottom dishes. The mitochondrial membrane potential was determined by staining with 50 nM of tetramethylrhodamine ethyl ester (Invitrogen) for 30 minutes at 37°C. To determine mitochondrial ROS production, cells were incubated with 0.3 mM MitoSOX Red (Invitrogen) for 15 minutes. Fluorescent images for the above experiments were collected using an Olympus FV3000 (Olympus, Tokyo, Japan), and the mean fluorescent intensity in the fluorescence-positive area was measured using ImageJ. More than five images were collected for each sample (>150 cells per sample). Relative quantification of mtDNA copy numbers was performed as described previously.[10]

Assessment of Autophagic Flux Index in Proximal Tubular Epithelial Cells

Autophagic flux was assessed by comparing MAP1LC3B levels with and without bafilomycin treatment as described previously.[13] The autophagic flux index is defined as the ratio of the MAP1LC3B-II level in the presence of bafilomycin A1 to that in the absence of bafilomycin A1.

Quantitative Reverse Transcription-PCR and Western Blot Analysis

Quantitative reverse transcription-PCR and western blot analyses were performed as described previously.[34] The sequences of the primers used are as follows: Mlxip (F5′-TGCTACCTGCCACAGGAGTC-3′, R5′-GACTCAAACAGTGGCTTGATGA-3′), Txnip (F5′-TCCTCAAGATGGGTGGCAAT-3′, R5′-CCGAGAAAGTGGTCAGGTCT-3′), Arrdc4 (F5′-CAGCCTCCTCAGAAGTGGAAT-3′, R5′-TCAGACGGAAGCTGAAAGCG-3′), Rubicon (F5′-CTCATCCATGACCAGGTGTG-3′, R5′-GTCGCTCTCATGCAAACTGA-3′), Pgc1a (F5′-TGATGTGAATGACTTGGATACAGACA-3′, R5′-GCTCATTGTTGTACTGGTTGGATATG-3′), Tfam (F5′-GCGCACGGGGGTCGAGATGT-3′, R5′-TGATAGACGAGGGGATGCGA-3′), Ndufa1 (F5′-ATTATGGGGGTGTGCTTGGT-3′, R5′-ATCGCGTTCCATCAGATACC-3′), Sdha (F5′-TTACCTGCGTTTCCCCTCAT-3′, R5′-AAGTCTGGCGCAACTCAATC-3′), Uqcr11 (F5′-ATGCTGAGCAGGTTTCTAGG-3′, R5′-CCTTCTTAAACTTGCCGTTG-3′), Cox4 (F5′-GCACCAATGAATGGAAGACA-3′, R5′-ATAGTCCCACTTGGCGGAGA-3′), Atp5o (F5′-GCACCGTCAAAGTGAAAAGC-3′, R5′-ATGCTGTGGTCACTGTGCAT-3′), Ctsd (F5′-TCAGGAAGCCTCTCTGGGTA-3′, R5′-CCCAAGATGCCATCAAACTT-3′), Ctsb (F5′-GGCTTTGACTGCAGGACTTC-3′, R5′-GACAGGACCAAGGAGAGCTG-3′), Lamp1 (F5′-GATGAATGCCAGCTCTAGCC-3′, R5′-CTGGACCTGCACACTGAAGA-3′), Hexa (F5′-ACATCTCGCCATTACCTGCC-3′, R5′-AAGAGTCGTCCACCAAGTGC-3′), Uvrag (F5′-ACTAAGACTCACATCGACAAGC-3′, R5′-GCGCTTTCTTCTGTCTTTCCAG-3′), Rragc (F5′-TTTCCTGGGCAGATGGACTTC-3′, R5′-ATATCAATGCTCCTGTGCCCC-3′), Rragd (F5′-GCCCCGTATGACAAGGACTC-3′, R5′-CTCTGACGAAGCAAACGAGC-3′), SQSTM1/p62 (F5′-CCCCAGAGTCGAAGTAGCTG-3′, R5′-AGTGAGAAGAGGCTGGTGGA-3′), Map1lc3b (F5′-ACAAAGAGTGGAAGATGTCCGGCT-3′, R5′-TGCAAGCGCCGTCTGATTATCTTG-3′), Gdf15 (F5′-AGTGTCCCCACCTGTATCG-3′, R5′-TGTCCTGTGCATAAGAACCA-3′), Mcoln1 (F5′-CCTACCATGTGAAGTTCCGCT-3′, R5′-TGTCGTCTCCGTTGATGAGTG-3′), Actb (F5′-TGACAGGATGCAGAAGGAGA-3′, R5′-ACATCTGCTGGAAGGTGGAC-3′), Col i (F5′-ACGCCATCAAGGTCTACTGC-3′, R5′-ACTCGAACGGGAATCCATCG-3′), Col iii (F5′-CAGCTGGCATTCCTGGAGCCC-3′, R5′-ACCAGCTTCGCCCCGTTCAC-3′), Fibronectin (F5′-ATACCGTTGTCCCAGAGGTG-3′, R5′-GGAAGAGTTTAGCGGGGTCC-3′), Havcr1/Kim1 (F5′-TCAGCTCGGGAATGCACA-3′, R5′-TGGTTGCCTTCCGTGTCT-3′), Lcn2/Ngal (F5′-GGCCAGTTCACTCTGGGAAA-3′, R5′-GGCGAACTGGTTGTAGTCC-3′).

Biochemical Parameters

Blood samples were collected from mice under anesthesia. Plasma was obtained after centrifugation (15 minutes, 3000×rpm, 4°C), and concentrations of plasma creatinine were determined using DICT-500 (BioAssay Systems, Hayward, CA), in accordance with the manufacturer's instructions.

Measurement of Mitochondrial Respiratory Function

The mitochondrial oxygen consumption rate (OCR) was measured using Seahorse XF96 analyzer (Seahorse Bioscience, North Billerica, MA) as described previously with slight modifications.[29,35] Briefly, proximal tubular epithelial cells in Seahorse XF DMEM, pH 7.4 (Agilent Technologies, Santa Clara, CA, 103578-100) supplemented with 10 mM glucose (Agilent Technologies, 103577-100), 1 mM pyruvate (Agilent Technologies, 103578-100), and 2 mM L-glutamine (Agilent Technologies, 103579-100) were stimulated with 1.5 μM oligomycin A, 1.0 μM trifluoromethoxy carbonylcyanide phenylhydrazone, and 0.5 μM rotenone and antimycin A using Seahorse XF Cell Mito Stress Test Kit (Agilent Technologies, 103015-100) to determine mitochondrial activity. OCR was analyzed with Wave software v2.6.1 (Agilent Technologies) and normalized to the total protein levels after the assay.

Kidney Biopsy Specimens

Human kidney specimens were obtained from patients who had undergone kidney biopsy at the Osaka University Hospital. Kidney biopsy specimens diagnosed with no significant abnormal changes or benign nephrosclerosis, which is

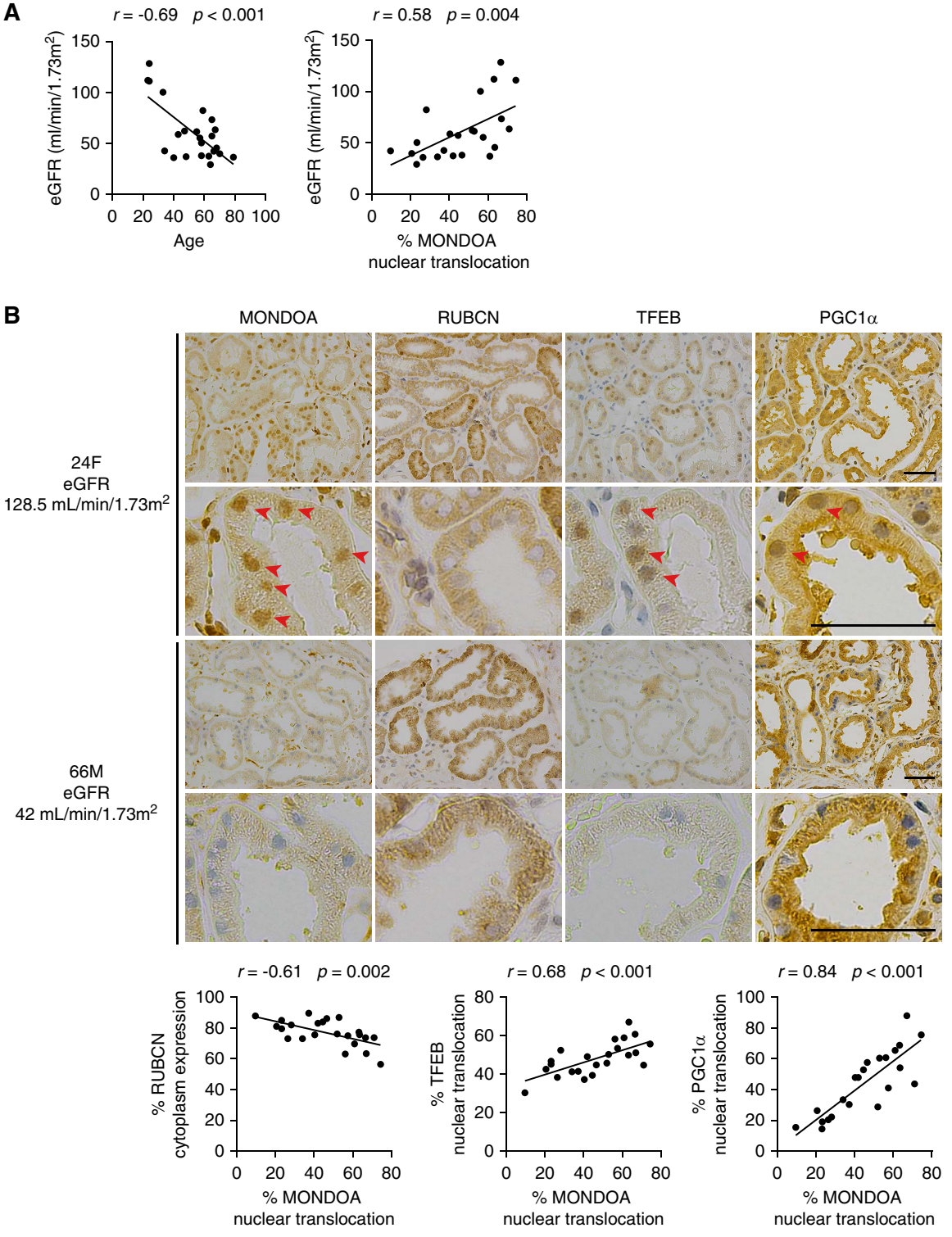

Figure 1. Nuclear MONDOA is decreased in proximal tubular epithelial cells of CKD patients. Correlation analysis between eGFR, age, nuclear MONDOA, and other downstream factors, using human kidney biopsy samples. (A) Correlation of eGFR with age (left) and the percentage of proximal tubular epithelial cells with nuclear MONDOA (right) (n=23). (B) Representative images of immunohistochemical staining for MONDOA, RUBCN, and TFEB in kidney biopsy samples of patients with CKD, each with the indicated age, sex, and eGFR (ml/min per 1.73 m^2). Specimens were counterstained with hematoxylin. Magnified images are shown in the lower panels. Bars: 50 μm. Correlation of the percentage of proximal tubular epithelial cells showing nuclear MONDOA translocation with the percentages of proximal tubular epithelial cells with each of the following: RUBCN in cytoplasm (left), nuclear TFEB (middle), and nuclear PGC1α (right). (A and B) Relationships were examined using Pearson correlation and the corresponding P values. PGC1α, peroxisome proliferator-activated receptor-γ coactivator-1α; RUBCN, run domain beclin-1–interacting and cysteine-rich domain-containing protein; TFEB, transcription factor EB.

the representative pathological finding in the aged kidneys.[36,37] Allograft biopsy specimens were derived at the time of kidney transplantation. The percentage of proximal tubular epithelial cells exhibiting MONDOA, TFEB, and PGC1α nuclear translocation and the percentage of the immune-positive area for RUBCN were assessed in at least five randomly selected high-power fields (×400) in the cortex. In all immunohistochemical studies, at least five high-power fields were reviewed by three nephrologists (S. Maeda, S. Sakai, and T. Yamamoto) in a blinded manner.

Statistical Analyses

All results are presented as bar graphs showing means±SEM. Statistical analyses were conducted using JMP software (SAS Institute). Multiple-group comparisons were performed using ANOVA with post-testing using the Tukey–Kramer test. The difference between any two experimental values was assessed using the Student t test when appropriate. A one-way ANOVA followed by the Dunnett test was used to detect intergroup differences. Statistical significance was defined as $P < 0.05$. Relationships were examined using Pearson correlation and the corresponding P values.

Study Approval

All animal experiments were approved by the Animal Research Committee of Osaka University and conformed to the Japanese Animal Protection and Management Law (No. 25). All human studies were approved by the Institutional Review Board of Osaka University Hospital (Institutional Review Board number 17334 and 20504) and adhered to the Declaration of Istanbul. The clinical and research activities being reported are consistent with the Principles of the Declaration of Istanbul as outlined in the Declaration of Istanbul on Organ Trafficking and Transplant Tourism. We have complied with all of the relevant ethical regulations, and informed consent was obtained.

Results

MONDOA Activity Was Decreased in Proximal Tubular Epithelial Cells of Patients with CKD

Our recent study showed that the levels of nuclear MONDOA were reduced in the kidneys of patients with ischemic AKI.[15] After confirming nuclear MONDOA staining in proximal tubular epithelial cells throughout the cortex of human kidney biopsy specimens (Supplemental Figure 1A), we first investigated the correlation between MONDOA and kidney function and factors associated with MONDOA in kidney biopsy specimens diagnosed with no significant abnormal changes or benign nephrosclerosis (Supplemental Table 1). The mean age and eGFR of the patients in this study were 53±16 years and 61±28 ml/min per 1.73 m^2, respectively, and there was a negative correlation between age and eGFR (Figure 1A and Supplemental Table 2). We observed a positive correlation between eGFR and the nuclear staining of MONDOA in proximal tubular epithelial cells (Figure 1A). In addition, we examined the expression of RUBCN and TFEB, both of which are downstream factors associated with MONDOA. RUBCN expression was correlated negatively with eGFR and nuclear MONDOA in proximal tubular epithelial cells (Figure 1B and Supplemental Figure 1, B and C). There was also a positive correlation between nuclear MONDOA and TFEB, and between nuclear TFEB and eGFR (Figure 1B and Supplemental Figure 1C). Collectively, these results suggest that MONDOA activity in proximal tubular epithelial cells may be decreased in patients with CKD, along with the downstream factor TFEB.

Transcriptional Activity of MondoA in Proximal Tubular Epithelial Cells Was Decreased under Hypoxic/Ischemic Conditions but Increased during Reoxygenation

We examined the time-dependent changes in MondoA transcriptional activity under hypoxic/ischemic conditions and during reoxygenation/reperfusion in proximal tubular epithelial cells. First, single-cell RNA sequencing transcriptomic analysis was performed by using data of mice subjected to bilateral IRI from a previous report.[24] In the report, a model of adaptive and maladaptive repair was established by carefully titrating renal ischemia time in mice: analysis of short IRI versus long IRI. The expression variability of Mlxip/MondoA gene and downstream factor genes was shown (Figure 2A and Supplemental Figure 2A). Mlxip/MondoA gene expression was suppressed and then gradually increased 1 day and 3–14 days post-long IRI, respectively, especially in the S3 segments of the proximal tubule (Figure 2A and Supplemental Figure 2B). Furthermore, Mlxip/MondoA mRNA expression in the kidney was suppressed 2 days post-unilateral IRI and then gradually increased at both 1 and 3 weeks (Figure 2B). The time-dependent changes in Arrdc4 and thioredoxin-interacting protein, both of which are downstream factors of MondoA, exhibited similar trends (Supplemental Figure 2C). To estimate the dynamics of MondoA transcriptional activity *in vitro*, we subjected cultured proximal tubular epithelial cells to H/R stress. The expression levels of MondoA, Txnip, and Arrdc4, but not Rubicon, were suppressed during hypoxia but were enhanced after reoxygenation in cultured proximal tubular epithelial cells (Figure 2, C and D). To investigate whether the above *in vitro* data were also relevant in humans, we compared the expression of MONDOA between kidney biopsy samples of human allografts obtained at the time of kidney transplantation and those of minor glomerular abnormalities. The expression of MONDOA was decreased in the human allograft biopsy samples (Figure 2E and Supplemental Table 3). Together, these results show that transcriptional activity of MondoA in proximal tubular epithelial cells is decreased under hypoxic/ischemic conditions but is increased during reoxygenation.

Decreased MondoA Transcriptional Activity Aggravated Kidney Injury and Impaired Autophagic Flux after IRI

To investigate the effects of suppressed MondoA transcriptional activity in proximal tubular epithelial cells during hypoxia/ischemia, we generated *MondoA*-deficient proximal tubular epithelial cells. Since MondoA functions as a glucose sensor,[17] 2DG drives MondoA activity by increasing glucose-6-phosphate levels.[17,18,20] We first used 2DG for the experiment to confirm the deficiency of MondoA. 2DG

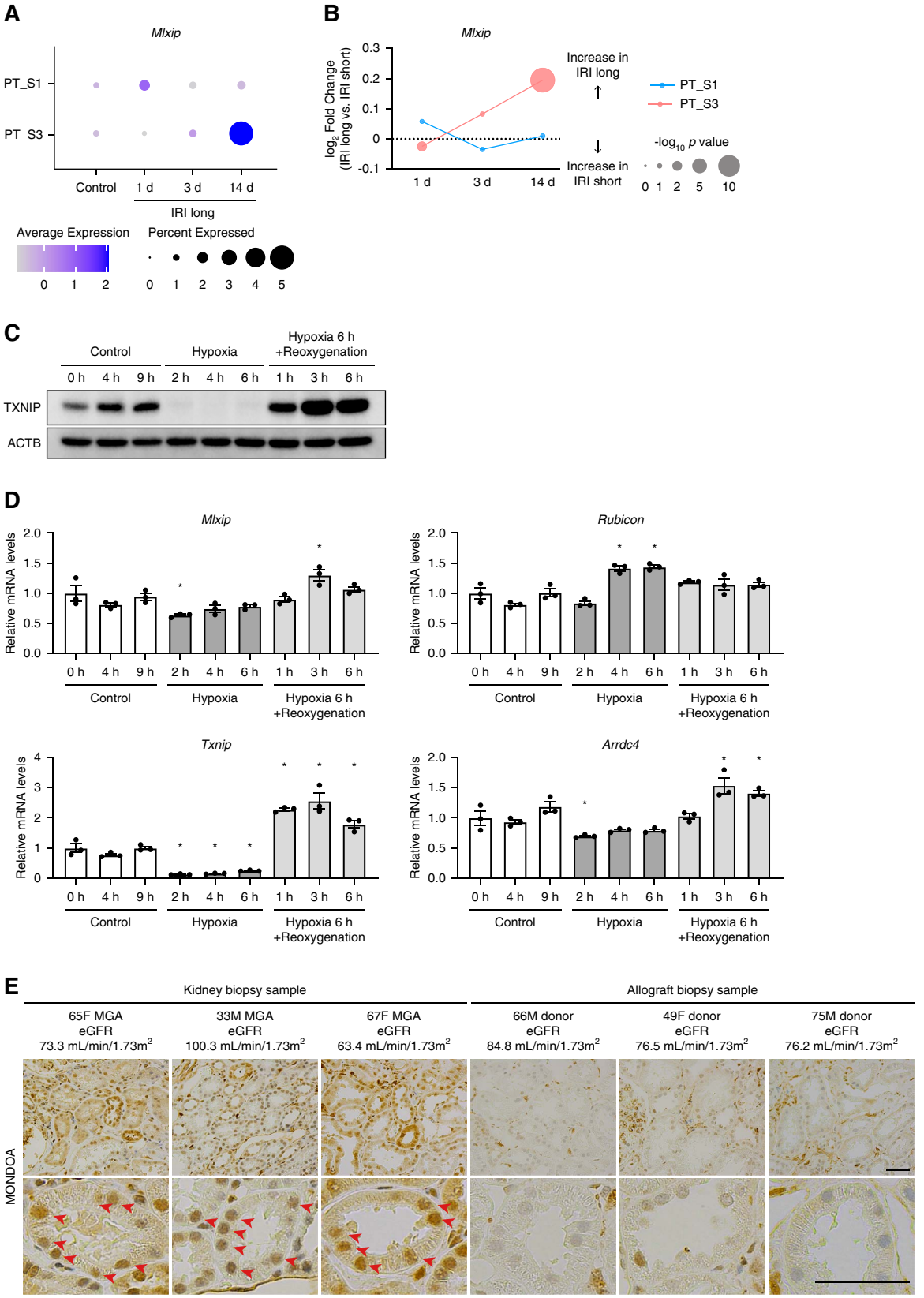

Figure 2. Transcriptional activity of MondoA decreases under ischemic conditions but increases during reoxygenation in proximal tubular epithelial cells. (A and B) scRNA-seq transcriptomic analysis was performed by using data of mice subjected to bilateral IRI in a previous study.[24] (A) Dot plot showing the scaled expression of *Mlxip/MondoA* in the proximal tubule segments at different time points after bilateral

Figure 2. *Continued.* long (30 minutes) IRI. PT S1 and PT S3 represent the S1 and S3 segments of the proximal tubule, respectively. The diameter of the dots corresponds to the percentage of cells expressing *Mlxip/MondoA*, and the density of the dots corresponds to the average expression for all proximal tubular epithelial cells in the dataset. (B) Differential gene expression analysis between long (30 minutes) IRI versus short (23 minutes) IRI in the S1 and S3 segments of the proximal tubule across time course. (C and D) The dynamics of MondoA transcriptional activity in cultured proximal tubular epithelial cells after H/R. The protein level of TXNIP (C) and the mRNA levels of *Mlxip*, *Rubicon*, *Txnip*, and *Arrdc4* (D) in cultured proximal tubular epithelial cells subjected to normoxia, hypoxia, or H/R for the indicated periods ($n=3$). (C) A representative western blot image. (D) mRNA levels normalized by those of cells cultured under normoxia for 0 hour. (E) Representative images of immunohistochemical staining for MONDOA in kidney biopsy samples of patients with CKD and allograft biopsy samples of donors, each with the indicated age, sex, and eGFR (ml/min per 1.73 m^2). Specimens were counterstained with hematoxylin. Magnified images are shown in the lower panels. Bars: 50 μm. Data are provided as means±SEM. Statistically significant differences: $^*P<0.05$ versus kidneys at 0 hour or proximal tubular epithelial cells cultured under normoxia for 0 hour (D, one-way ANOVA followed by Dunnett test). Arrdc4, arrestin domain containing 4; H/R, hypoxia/reoxygenation; IRI, ischemia-reperfusion injury; MGA, minor glomerular abnormalities; MLXIP, MLX interacting protein; PT, proximal tubule; scRNA-seq, single-cell RNA sequencing; TXNIP, thioredoxin-interacting protein.

treatment induced a significant increase in the expression of MondoA, Arrdc4, and Txnip in wild-type proximal tubular epithelial cells, and in each case, this expression was completely abolished by *MondoA* deficiency (Supplemental Figure 3, A and B). Then, we subjected wild-type and *MondoA*-deficient proximal tubular epithelial cells to H/R stress (6 hours of hypoxia followed by 3 hours of reoxygenation) with low-glucose medium. Notably, a significant increase in the expression of Rubicon and SQSTM1/p62 was observed in *MondoA*-deficient proximal tubular epithelial cells but not in wild-type proximal tubular epithelial cells (Figure 3A). Indeed, autophagic flux, as assessed by differences in MAP1LC3B-II levels with and without bafilomycin A treatment, was severely impaired in *MondoA*-deficient proximal tubular epithelial cells subjected to H/R stress (Figure 3B). Furthermore, an immunofluorescence study of LC3 and LAMP1 revealed that the numbers of autophagosomes, lysosomes, and autolysosomes were decreased at baseline, and the increases in their numbers after H/R stress were abolished in *MondoA*-deficient proximal tubular epithelial cells, indicating that MondoA contributes to autophagy initiation and autophagosome maturation (Supplemental Figure 3C).

Next, to investigate the role of MondoA in IRI, 8-week-old $MondoA^{F/F}$ mice and $MondoA^{F/F}$; KAP mice deficient in proximal tubule–specific *MondoA* were subjected to unilateral IRI. MondoA gene expression was decreased in both sham-operated and IRI *MondoA*-deficient kidneys (Supplemental Figure 4A). Periodic acid–Schiff staining demonstrated severely injured tubules with vacuolation and massive tubular dilation with casts in the kidney cortex of IRI $MondoA^{F/F}$; KAP mice compared with $MondoA^{F/F}$ controls (Figure 3C). IRI *MondoA*-deficient kidneys exhibited significant increases in the mRNA levels of the tubular injury markers *Havcr1/Kim-1* and *Lcn2/Ngal* (Figure 3D). The number of TUNEL-positive tubular cells was prominently increased in IRI *MondoA*-deficient kidneys (Supplemental Figure 4B). Notably, bilateral IRI induced a significant increase in plasma creatinine in $MondoA^{F/F}$; KAP mice compared with $MondoA^{F/F}$ mice (Supplemental Figure 4C). Moreover, the expression of Rubicon and SQSTM1/p62 was increased in IRI kidneys of $MondoA^{F/F}$; KAP mice, indicating that autophagy flux is disturbed in *MondoA*-deficient kidneys during ischemic AKI (Figure 3E). To precisely assess autophagic flux *in vivo*, GFP-MAP1LC3 transgenic $MondoA^{F/F}$ and $MondoA^{F/F}$; KAP mice at 12 hours post-IRI were administered CQ, an inhibitor of lysosomal acidification, 6 hours before euthanasia.[10] GFP-positive dots representing autophagosomes were rarely observed in CQ-free $MondoA^{F/F}$ and $MondoA^{F/F}$; KAP mice, and the numbers of these dots remained unchanged by CQ administration, suggesting that the autophagic activity in both types of mice is low under physiological conditions. By contrast, a substantial number of dots were observed in proximal tubular epithelial cells of CQ-free IRI $MondoA^{F/F}$ and $MondoA^{F/F}$; KAP mice. CQ administration significantly increased the number of dots in $MondoA^{F/F}$ mice, whereas this number remained unchanged in $MondoA^{F/F}$; KAP mice; this suggests that autophagic flux was enhanced in $MondoA^{F/F}$ mice after IRI, but was impaired in *MondoA*-deficient kidneys (Figure 3F). In IRI kidneys of $MondoA^{F/F}$; KAP mice, electron microscopy revealed a decrease in the number of autophagosomes and severe abnormalities in mitochondrial morphology (Figure 3G). On the other hand, necrosis was comparable in both groups of IRI $MondoA^{F/F}$ and $MondoA^{F/F}$; KAP mice (Supplemental Figure 4D). Recent study findings, including single cell-based transcriptomics, revealed that VCAM1-positive failed-repair proximal tubular epithelial cells are inflammatory proximal tubules that fail to regenerate after IRI.[38] Increased VCAM1 expression together with SQSTM1/p62 was observed in the proximal tubular epithelial cells of IRI $MondoA^{F/F}$; KAP mice compared with IRI $MondoA^{F/F}$ mice (Supplemental Figure 4E). Collectively, these findings indicate that decreased MondoA transcriptional activity aggravates kidney injury and impairs autophagic flux after IRI.

Loss of *MondoA* Exacerbated Hypoxia/Ischemia-Induced Mitochondrial Dysfunction

Next, since *MondoA* deficiency caused impaired autophagy flux and abnormalities in mitochondrial morphology, we examined the role of MondoA in mitochondrial function in cultured proximal tubular epithelial cells. Loss of *MondoA* in proximal tubular epithelial cells, in response to H/R, led to decreased mitochondrial membrane potentials and increased mitochondrial ROS, as assessed by tetramethylrhodamine ethyl ester and MitoSOX staining, respectively (Figure 4, A and B). Mitochondrial respiration activity, as assessed by SDH staining, was consistently somewhat decreased in the kidneys of IRI $MondoA^{F/F}$ mice compared with sham-operated kidneys, whereas a more prominent decline was observed in *MondoA*-deficient kidneys

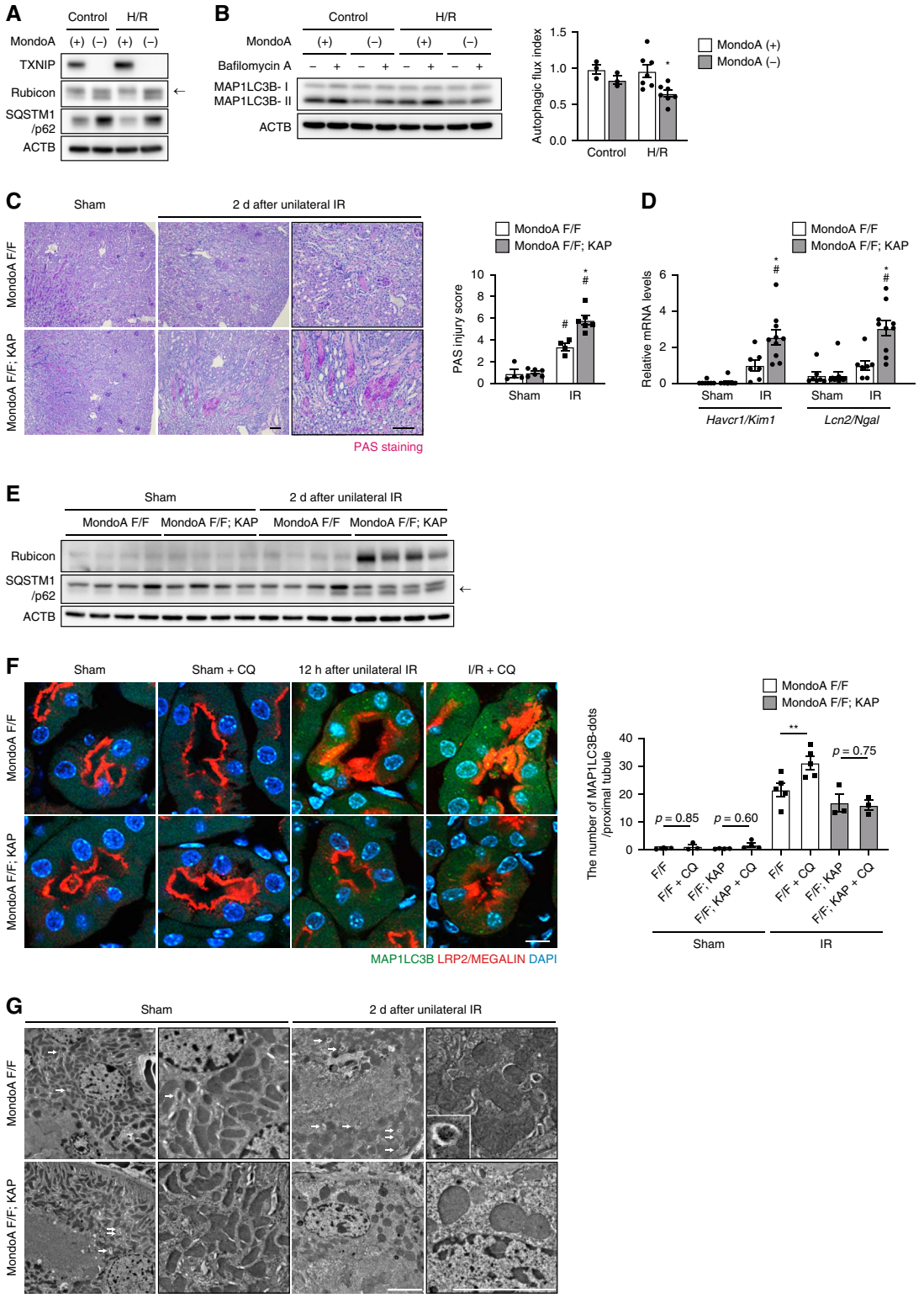

Figure 3. Loss of *MondoA* increases Rubicon and impairs autophagic flux in proximal tubular epithelial cells during IR. The effect of MondoA deficiency on autophagic flux and cell injury during IR or H/R was investigated using *MondoA*-deficient mice and cultured proximal tubular epithelial cells. (A and B) Wild-type and *MondoA*-deficient proximal tubular epithelial cells were subjected to H/R. (A) Western blot images of TXNIP, Rubicon, and SQSTM1/p62. Arrow indicates Rubicon-specific band. (B) Western blot images of MAP1LC3B in proximal tubular epithelial cells incubated with or without bafilomycin A1 are presented. The autophagic flux index was assessed (n=3–7 per group). (C–E) *MondoA*$^{F/F}$ and *MondoA*$^{F/F}$; KAP mice were subjected to a sham operation or unilateral IRI. Images are shown for PAS staining (C), mRNA levels of *Havcr1/Kim-1* and *Lcn2/Ngal* (D), and western blot analysis of Rubicon and SQSTM1/p62 (E) in the kidney cortical regions of IRI mice 2 days after unilateral IRI. (C) The tubular injury score is shown (n=4–6 per group) and (D) n=7–10 per

Figure 3. *Continued.* group. (E) Arrow indicates SQSTM1/p62-specific band. (F) Autophagic flux was assessed by counting the number of GFP-positive dots in the proximal tubules of GFP-MAP1LC3 transgenic *MondoA*$^{F/F}$ or *MondoA*$^{F/F}$; KAP mice with or without CQ administration; analysis was performed either after sham-operation or 12 hours after IRI (n=3–4 in the sham-operated group and 3–5 in the IRI group). The number of GFP-positive dots per proximal tubule under each condition was counted in at least ten high-power fields (original magnification, ×600), with each high-power field containing 10–15 proximal tubules. (G) Images of electron micrographs of the kidneys of IRI mice 2 days after unilateral IRI. Arrows indicate autophagosomes. (A, B, and E) ACTB was used as loading control. (A, B, C, F, and G) Representative images are presented. Magnified images are shown in the insets. Bars: 100 μm (C), 10 μm (F), and 5 μm (G). Data are provided as means±SEM. Statistically significant differences: $^{*}P < 0.05$ versus treatment matched wild-type proximal tubular epithelial cells or *MondoA*$^{F/F}$ control littermates; $^{\#}P < 0.05$ versus sham-operated kidney in each group; $^{**}P < 0.05$ versus mice with no CQ treatment (B–D, one-way ANOVA followed by Tukey–Kramer test; F, Student t test). Control, normoxia-treated controls; MondoA (+), wild-type proximal tubular epithelial cells; MondoA (−), *MondoA*-deficient proximal tubular epithelial cells; MondoA F/F, *MondoA*$^{F/F}$ mice; MondoA F/F; KAP, *MondoA*$^{F/F}$; KAP mice. ACTB, actin beta; CQ, chloroquine; DAPI, 4′,6-diamidino-2-phenylindole; GFP, green fluorescent protein; IR, ischemia-reperfusion; KAP, kidney androgen-regulated protein-Cre; PAS, Periodic acid–Schiff; SQSTM1, sequestosome 1.

(Figure 4C). Although MondoA delays doxorubicin-induced cellular senescence in human retinal pigment epithelial cells by maintaining mitochondrial function *via* upregulation of Prdx3,[15] no significant differences in Prdx3 levels were observed in proximal tubular epithelial cells regardless of MondoA expression (Supplemental Figure 5). These data suggest that loss of *MondoA* exacerbates hypoxia/ischemia-induced mitochondrial dysfunction.

Ablation of *Rubicon* in *MondoA*-Deficient Kidneys Restored Autophagic Activity and Mitochondrial Function

Next, to test whether the impaired autophagic flux and mitochondrial dysfunction observed in *MondoA*-deficient proximal tubular epithelial cells were mediated by Rubicon, we knocked down *MondoA* in *Rubicon*-deficient proximal tubular epithelial cells (Supplemental Figure 6, A and B). *Rubicon* depletion increased the autophagic flux in *MondoA*-knocked down proximal tubular epithelial cells, as assessed by the difference in MAP1LC3B-II with and without bafilomycin A treatment (Figure 5A). In addition, to investigate the role of increased Rubicon in IRI *MondoA*-deficient kidneys, we newly generated proximal tubule–specific *MondoA*-deficient and *Rubicon*-deficient *MondoA*$^{F/F}$; *Rubicon*$^{F/F}$; KAP (double knockout [DKO]) mice and subjected them to IRI. The protein levels of Rubicon and SQSTM1/p62 were decreased in IRI DKO mouse kidneys (Figure 5B). Periodic acid–Schiff and SDH staining and electron microscopy demonstrated that compared with *MondoA*$^{F/F}$; KAP mice, DKO mice showed significant improvements in tubular injury, mitochondrial function, and autophagosome maturation in IR kidneys (Figure 5, C–E). IRI DKO mouse kidneys exhibited significant decreases in the mRNA levels of the tubular injury markers *Havcr1/Kim-1* and *Lcn2/Ngal* (Supplemental Figure 6C). Thus, ablation of *Rubicon* in *MondoA*-deficient kidneys restores autophagic activity and mitochondrial function.

Loss of *MondoA* during the Recovery Phase after IR Aggravated Kidney Injury with Downregulation of the TFEB-PGC1α Axis

Next, on the basis of the dynamics of MondoA, we hypothesized that MondoA reactivation 1-week post-IRI plays a protective role during the recovery phase after AKI and prevents the AKI-to-CKD transition. To test this hypothesis, we newly generated tamoxifen-inducible proximal tubule–specific *MondoA*-deficient mice. Tamoxifen was administered 1 and 4 days after the IR operation, and the time-dependent reduction in MondoA expression was confirmed in *MondoA*-deficient kidneys from 5 days to 3 weeks post-IRI (Figure 6, A and B). SDH and Masson trichrome staining, immunostaining for COL1A1, and mRNA levels of fibrosis markers demonstrated that loss of *MondoA* during the recovery phase after IRI led to mitochondrial dysfunction, more severe tubular injury, and interstitial fibrosis 3 weeks post-IRI (Figure 6, C–E, and Supplemental Figure 7, A and B). Next, we explored the mechanism by which MondoA reactivation protects against AKI-to-CKD transition by focusing on TFEB and mTOR kinase complex 1 (mTORC1) because in *Caenorhabditis* elegans, MondoA is required for the activation of TFEB, a central regulator of lysosome biogenesis and autophagy, and MondoA is also known to inhibit the mTORC1 and enhance TFEB activity.[19,39] In *MondoA*-deficient kidneys, TFEB nuclear translocation was significantly inhibited, and the protein levels of pRPS6, a downstream target of mTOR activity, were upregulated (Figure 6F and Supplemental Figure 7, C and D). We next focused on PGC1α, a known key regulator of mitochondrial biogenesis, as PGC1α cis-regulatory region bears the coordinated lysosomal expression and regulation motif, thereby allowing direct regulation by TFEB.[39–41] PGC1α expression and mRNA levels of mitochondria-related genes were significantly reduced 1 week post-IRI in *MondoA*-deficient kidneys (Figure 6G and Supplemental Figure 7E). Similarly, hyperactivation of the mTORC1 pathway and downregulation of the TFEB-PGC1α axis were observed in cultured *MondoA*-deficient proximal tubular epithelial cells after H/R (Supplemental Figure 7, F–H). Collectively, loss of *MondoA* during the recovery phase after IR aggravates kidney injury with downregulation of the TFEB-PGC1α axis. Moreover, analysis of human kidney biopsy samples showed that nuclear PGC1α correlated positively with nuclear MONDOA and eGFR (Figure 1B, Supplemental Figure 1, B and C). Together, these results indicate that MondoA is associated with the TFEB-PGC1α axis in both mice and humans.

Pharmacological Upregulation of the TFEB-PGC1α Axis Mitigated the AKI-to-CKD Transition in *MondoA*-Deficient Kidneys

Finally, we assessed whether pharmacological upregulation of the TFEB-PGC1α axis during the recovery phase could

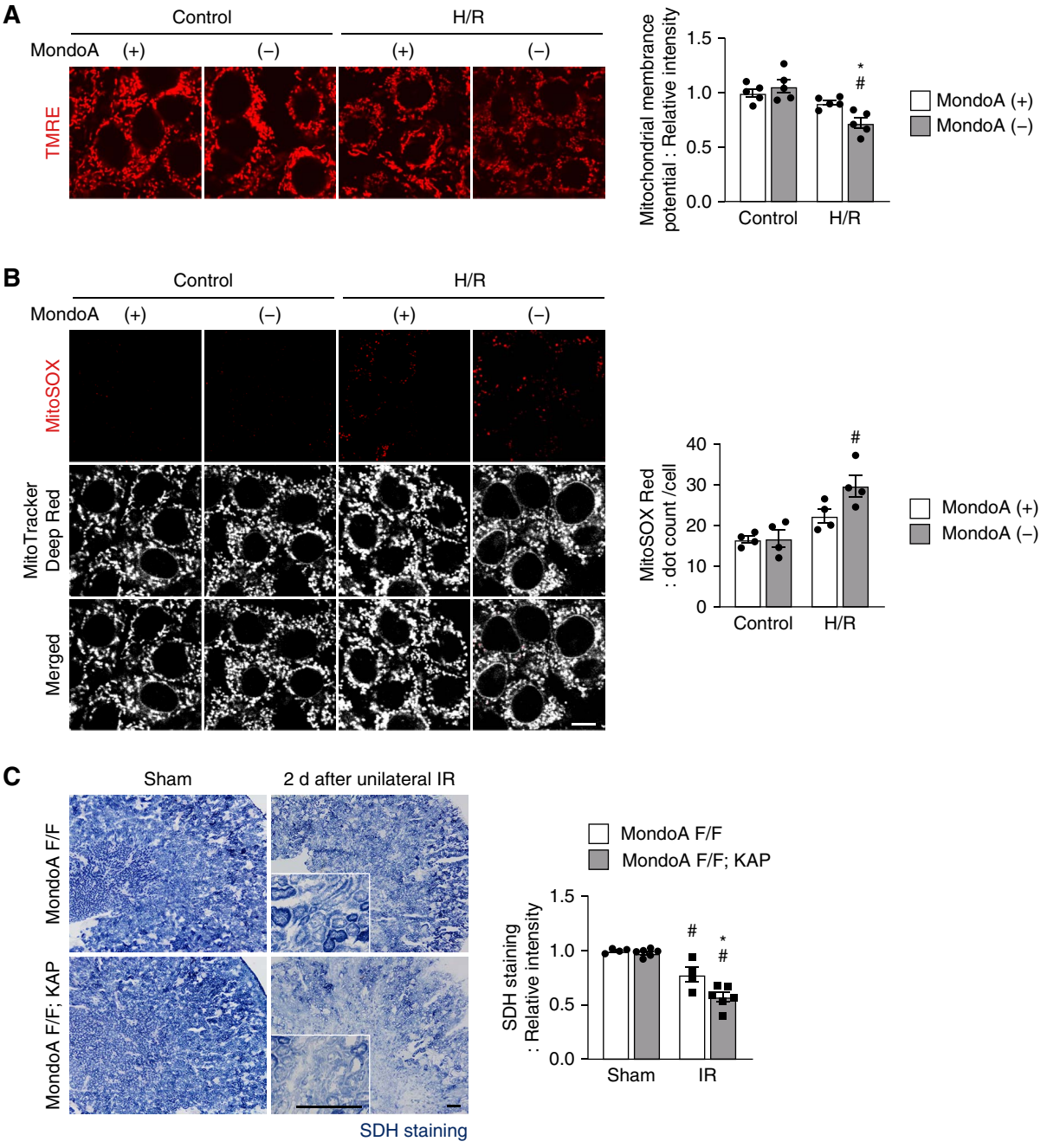

Figure 4. Loss of *MondoA* exacerbates H/R or IR-induced mitochondrial dysfunction in proximal tubular epithelial cells. The mitochondrial membrane potential (A) and the ROS production (B) of wild-type or *MondoA*-deficient proximal tubular epithelial cells subjected to H/R were assessed by TMRE and MitoSOX Red staining, respectively. Quantitative data of relative intensity are shown. More than 150 cells were quantified under each condition. (C) Representative images of SDH staining in the kidney cortical regions of *MondoA*$^{F/F}$ control and *MondoA*$^{F/F}$; KAP mice 2 days after sham operation or unilateral IRI (n=4–6 in each group). The relative staining intensity is shown. (A and C) The mean values for wild-type proximal tubular epithelial cells without H/R and for the sham-operated kidney cortical regions of *MondoA*$^{F/F}$ mice are expressed as 1. Magnified images are shown in the insets. Bars: 10 μm (A and B) and 200 μm (C). Data are provided as means±SEM. Statistically significant differences: $^{*}P < 0.05$ versus treatment-matched wild-type proximal tubular epithelial cells or *MondoA*$^{F/F}$ control littermates; $^{\#}P < 0.05$ versus normoxia-treated proximal tubular epithelial cells or sham-operated kidneys in each group (A–C, one-way ANOVA followed by Tukey–Kramer test). Control, normoxia-treated controls; MondoA (+), wild-type proximal tubular epithelial cells; MondoA (−), *MondoA*-deficient proximal tubular epithelial cells; MondoA F/F, *MondoA* $^{F/F}$ mice; MondoA F/F; KAP, *MondoA* $^{F/F}$; KAP mice. ROS, reactive oxygen species; SDH, succinate dehydrogenase; TMRE, tetramethylrhodamine ethyl ester.

mitigate the AKI-to-CKD transition in tamoxifen-induced *MondoA*-deficient mice. Trehalose, a natural disaccharide (α,α-1,1-glucoside) that has been reported to enhance TFEB nuclear translocation,[22] increased TFEB nuclear translocation as shown in western blot analysis and an immunofluorescence study and also increased the expression of *Tfeb*

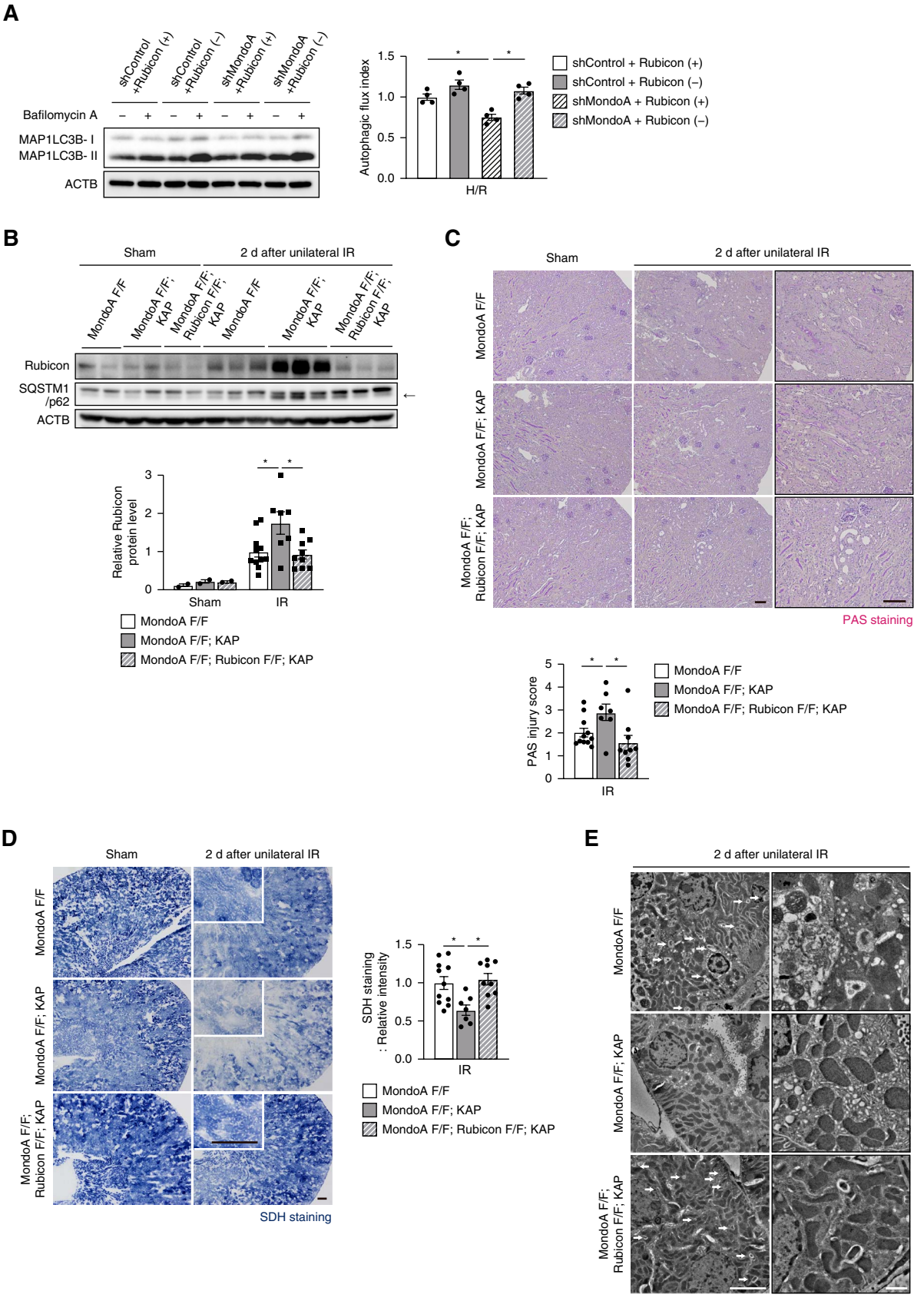

Figure 5. Loss of *Rubicon* in *MondoA*-deficient mice alleviates IRI by restoring autophagic activity. The effect of genetic ablation of *Rubicon* on IRI was investigated in *MondoA*-deficient kidneys. (A) Wild-type or *Rubicon*-deficient proximal tubular epithelial cells were knocked down for *MondoA* by shRNA, followed by H/R. Western blot images of MAP1LC3B in proximal tubular epithelial cells incubated

Figure 5. *Continued.* with or without bafilomycin A1 are presented. The autophagic flux index was assessed (n=4 per group). (B–E) *MondoA*$^{F/F}$, *MondoA*$^{F/F}$; KAP, and *MondoA*$^{F/F}$;*Rubicon*$^{F/F}$; KAP (DKO) mice were subjected to unilateral IRI. (B) Representative western blot images of Rubicon and SQSTM1/p62. Arrow indicates SQSTM1/p62-specific band. The relative amount of Rubicon protein was determined by densitometric analysis. Representative images of PAS (C) and SDH (D) staining and electron micrographs (E) of kidney cortical regions 2 days after unilateral IRI (n=7–11 per group). The tubular injury score (C) and the relative staining intensity (D) are shown. (E) Arrows indicate autophagosomes. Magnified images are shown in the insets. Bars: 100 μm (C), 200 μm (D), 5 μm (E, left), and 1 μm (E, right). Data are provided as means±SEM. (B and D) The mean value for IRI kidney cortical regions of *MondoA*$^{F/F}$ mice is expressed as 1. Statistically significant differences: *$P < 0.05$ versus *MondoA*-deficient and Rubicon-expressing proximal tubular epithelial cells or *MondoA*$^{F/F}$; KAP mice (A, one-way ANOVA followed by Tukey–Kramer test; B–D, Student t test). Rubicon (−), *Rubicon*-deficient proximal tubular epithelial cells; MondoA F/F, *MondoA*$^{F/F}$ mice; MondoA F/F; KAP, *MondoA*$^{F/F}$; KAP mice; MondoA F/F; Rubicon F/F; KAP, *MondoA*$^{F/F}$; *Rubicon*$^{F/F}$; KAP (DKO) mice. DKO, double knockout; shRNA, short hairpin RNA.

target genes in cultured proximal tubular epithelial cells regardless of MondoA expression (Figure 7, A and B and Supplemental Figure 8A). Next, *MondoA*$^{F/F}$ and *MondoA*$^{F/F}$; NDRG1 mice were subjected to sham operation or unilateral IRI, followed by intraperitoneal injection of tamoxifen and vehicle or trehalose (Supplemental Figure 8B). Trehalose administration induced TFEB nuclear translocation in IR-subjected, tamoxifen-inducible, proximal tubule–specific *MondoA*-deficient mice (Figure 7C). Furthermore, PGC1α expression was increased by trehalose both in *MondoA*$^{F/F}$ and *MondoA*$^{F/F}$; NDRG1 mice (Figure 7D and Supplemental Figure 8C). Trehalose mitigated tissue damage, kidney fibrosis, and mitochondrial dysfunction 3 weeks post-IR in *MondoA*$^{F/F}$; NDRG1 mice (Figure 7, E–G and Supplemental Figure 8, D and E). We next performed experiments using ZLN005, a PGC1α activator. It has been reported to protect progression of CKD by activating PGC1α pathway in ischemic nephropathy.[42,43] ZLN005 treatment increased the mRNA levels of *Pgc1α* in cultured proximal tubular epithelial cells regardless of MondoA expression (Supplemental Figure 9A). ZLN005 administration improved kidney fibrosis and mitochondrial dysfunction 3 weeks post-IR in *MondoA*$^{F/F}$; NDRG1 mice (Supplemental Figure 9, B–E). Mitochondrial DNA copy numbers were significantly reduced in *MondoA*-deficient kidneys 3 weeks post-IRI, while they improved with Trehalose and ZLN005 treatment (Supplemental Figure 9F). These findings suggest that reactivation of MondoA after IRI mitigates the AKI-to-CKD transition by upregulating the TFEB-PGC1α axis.

Discussion

In this study, we found that MONDOA activity in the proximal tubular epithelial cells of patients with CKD decreased in parallel with reduced eGFR and that hypoxia strongly reduced MONDOA nuclear localization in human kidneys. In addition, we demonstrated that MondoA protected against AKI and the AKI-to-CKD transition by two different mechanisms, depending on the phase after IRI: in the acute phase, MondoA suppressed Rubicon, which improves autophagy and maintains mitochondrial integrity, consequently alleviating AKI; by contrast, during the recovery phase, MondoA reactivation counteracted the AKI-to-CKD transition by increasing mitochondrial biogenesis *via* the TFEB-PGC1α axis, thereby promoting tubular recovery. These mechanisms may explain the vulnerability to AKI and the increased risk of disease progression in patients with CKD. A simple schematic drawing is shown in Figure 8.

Our extensive analysis of human kidney samples showed that MONDOA expression in proximal tubular epithelial cells decreased with declining eGFR and was also diminished under ischemic conditions. Given that the kidneys are susceptible to hypoxic conditions in patients with CKD,[44,45] hypoxia emerges as a common factor contributing to the reduced MondoA activity observed across these pathological states, as illustrated in Figure 8. The hypoxia-induced alterations in glucose and lipid metabolism and intracellular pH[46] may influence MondoA expression in a complex manner, because MondoA, acting as a glucose-sensing transcription factor,[17] orchestrates intricate cellular metabolic processes, including glycolysis and cell growth.[47,48] Indeed, loss of *MondoA* in proximal tubular epithelial cells led to mitochondrial dysfunction as assessed by OCR (Supplemental Figure 10A). Considering that MondoA also influences the expression of PGC1α, a crucial factor in metabolic pathways, future investigations should explore the complicated relationship between hypoxia, MondoA decline, and defective metabolism in kidney diseases.

Our observation of diminished MONDOA expression in patients with CKD implies that the insights obtained from genetically engineered, proximal tubule–specific, *MondoA*-deficient mouse models are applicable for clarifying the pathophysiology of patients with CKD. Here, we have uncovered the pivotal role of MondoA in suppressing Rubicon during the acute phase after IRI. Ablation of *Rubicon* in *MondoA*-deficient kidneys restored autophagic activity and mitochondrial function, demonstrating that Rubicon inhibition may be crucial for reducing the vulnerability to AKI, especially in patients with CKD, as illustrated in Figure 8. Furthermore, accumulating evidence has shown that suppressing excessive Rubicon could be protective in diverse pathological conditions such as nonalcoholic fatty liver disease, myocardial IRI, diabetic nephropathy, and organismal aging,[49–52] making Rubicon an attractive therapeutic target for a variety of age-related diseases. Our study highlighted the role of MondoA in suppressing Rubicon in proximal tubular epithelial cells (Figure 1B), although the detailed mechanism by which Rubicon expression levels are regulated requires further investigation in the future.

Another important finding is that MondoA activity retains its significance during the recovery phase. Induced deletion of

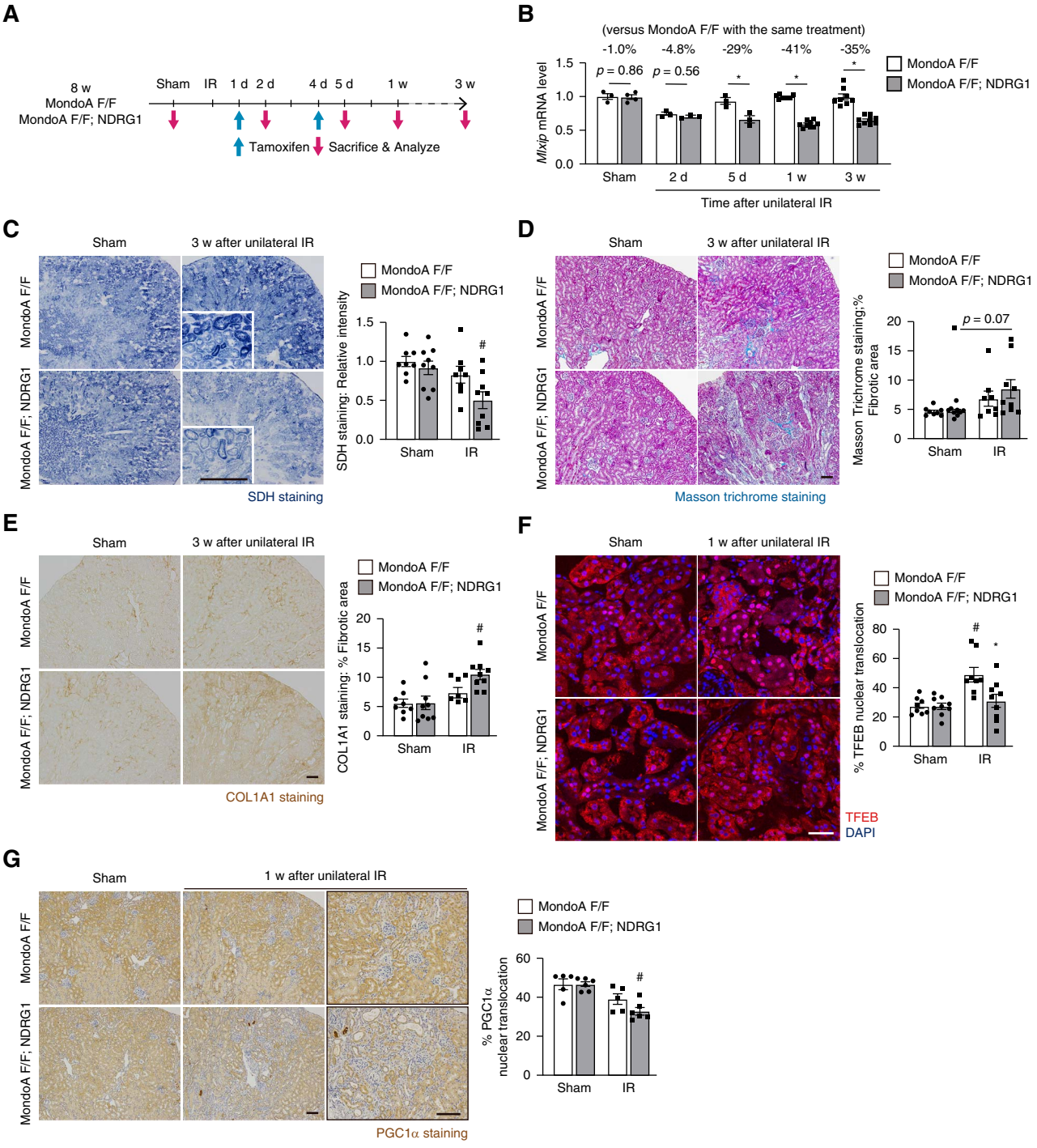

Figure 6. MondoA reactivation counteracts the AKI-to-CKD transition *via* the TFEB-PGC1α axis. To genetically inhibit MondoA reactivation, *MondoA*$^{F/F}$ and *MondoA*$^{F/F}$; NDRG1 mice were subjected to a sham operation or unilateral IRI, followed by intraperitoneal tamoxifen injection 1 and 4 days after the operation. (A) Experimental protocol. Kidneys were harvested and assessed at the indicated time points after IRI. (B) The mRNA levels of *Mlxip/MondoA* in kidney cortical regions are shown at the indicated time points after IRI (n=3–4 [sham, 2 and 5 days], and 7–9 [1 and 3 weeks]). (C–G) Representative images of SDH staining (C), Masson trichrome staining (D), and immunostaining for COL1A1 (E), TFEB (red) (F), and PGC1α (G) in kidney cortical regions either 1 (F and G) or 3 (C–E) weeks after the operation (n=8–9 in each group (C–F), n=5–6 in each group (G). (C) The relative intensity of SDH was assessed in at least five high-power fields (×400). The mean value for the sham-operated kidney of *MondoA*$^{F/F}$ mice is expressed as 1. (E) The COL1A1-positive area was assessed as a percentage in at least five high-power fields (×200). (F) Kidney sections were counterstained with DAPI (blue). The percentage of proximal tubular epithelial cells with TFEB nuclear translocation was counted in at least ten high-power fields (×600). (G) Sections were counterstained with hematoxylin. Magnified images are shown in the insets. Bars: 200 μm (C), 100 μm (D, E, and G), and 40 μm (F). Data are provided as means±SEM. Statistically significant differences: $^{*}P<0.05$ versus treatment-matched *MondoA*$^{F/F}$ control littermates; $^{\#}P<0.05$ versus sham-operated kidney in each group (B, Student *t* test; C–G, one-way ANOVA followed by Tukey–Kramer test). MondoA F/F, *MondoA*$^{F/F}$ mice; MondoA F/F; NDRG1, *MondoA*$^{F/F}$; NDRG1 mice. NDRG1, *N*-myc downstream-regulated gene 1.

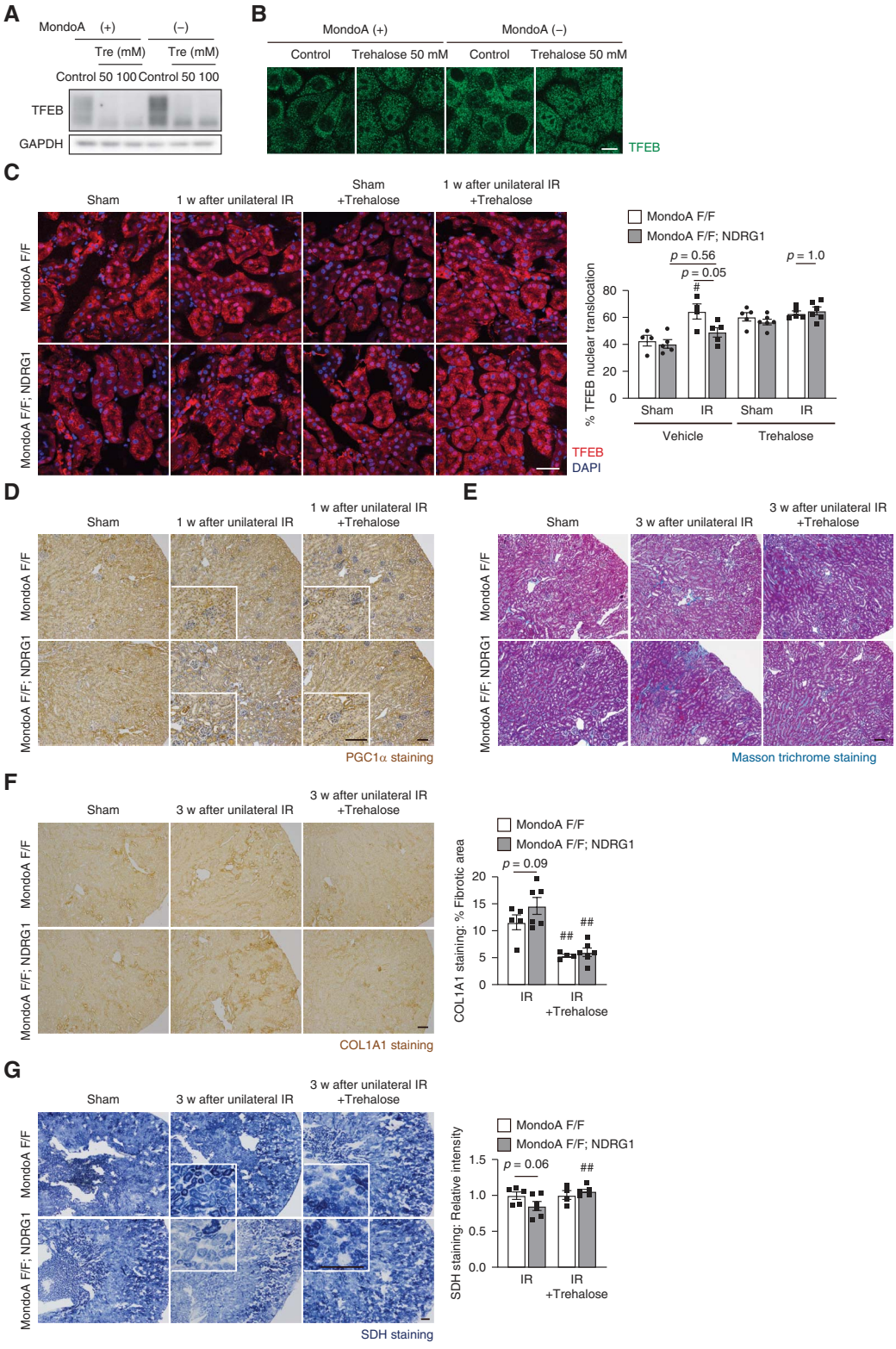

Figure 7. Pharmacological upregulation of the TFEB-PGC1α axis mitigates the AKI-to-CKD transition in *MondoA*-deficient kidneys. (A and B) Wild-type and *MondoA*-deficient proximal tubular epithelial cells were cultured with or without the indicated concentrations of trehalose. Representative images of western blot analysis (A) and immunofluorescence staining (B) of TFEB. (C–G) *MondoA*$^{F/F}$ and *MondoA*$^{F/F}$; NDRG1 mice were subjected to a sham operation or unilateral IRI, followed by injections of tamoxifen 1 and 4 days after the operation and trehalose three times a week. Representative images of immunostaining for TFEB (red) (C) and PGC1α (D), Masson trichrome staining (E), immunohistochemical staining for COL1A1 (F), and SDH staining (G) in kidney cortical regions were obtained 1 (C and D) or 3 (E–G) weeks after the operation with or without trehalose treatment (n=4–6 per group). (C) Kidney sections were counterstained with DAPI (blue). The percentage of

Figure 7. *Continued.* proximal tubular epithelial cells with TFEB nuclear translocation was counted in at least ten high-power fields (×600). (D and F) Sections were counterstained with hematoxylin. (F) The COL1A1-positive area was assessed as a percentage in at least five high-power fields (×200). (G) The relative intensity of SDH was assessed in at least five high-power fields (×400). The mean value for the IRI kidney cortical regions of *MondoA*$^{F/F}$ mice is expressed as 1. Magnified images are shown in the insets. Bars: 10 μm (B), 40 μm (C), 100 μm (D–F), and 200 μm (G). Data are provided as means±SEM. Statistically significant differences: $^{\#}P < 0.05$ versus sham-operated kidney in each group; $^{\#\#}P < 0.05$ versus IRI kidney in each group (C, F, and G, one-way ANOVA followed by Tukey–Kramer test). MondoA (+), wild-type proximal tubular epithelial cells; MondoA (−), *MondoA*-deficient proximal tubular epithelial cells; control, without trehalose; Tre, trehalose; MondoA F/F, *MondoA*$^{F/F}$ mice; MondoA F/F; NDRG1, *MondoA*$^{F/F}$; NDRG1 mice. GAPDH, glyceraldehyde-3-phosphate dehydrogenase.

MondoA in proximal tubular epithelial cells after AKI exacerbated mitochondrial dysfunction, tubular injury, and interstitial fibrosis 3 weeks post-IRI, demonstrating that MondoA reactivation counteracts the AKI-to-CKD transition, as illustrated in Figure 8. Mechanistically, we found that tubular recovery is promoted by mitochondrial biogenesis *via* the TFEB-PGC1α axis. Current studies present conflicting information on the role of autophagy during the recovery phase, some demonstrating that it slows CKD progression [53,54] and others reporting that it exacerbates CKD progression.[55,56] By contrast, PGC1α has emerged as a pivotal factor in mitochondrial biogenesis during the recovery phase,[57,58] with roles in regulating fatty acid beta-oxidation, maintaining mitochondrial function,[59] and exerting mutual transcriptional control with TFEB.[60–62] Indeed, pharmacological upregulation of the TFEB-PGC1α axis was sufficient to mitigate CKD progression in *MondoA*-deficient kidneys, making the TFEB-PGC1α axis an attractive therapeutic target as well. Our findings clearly show that MondoA is generally protective against AKI and the AKI-to-CKD transition.

As there remains a possibility that the interrelationship of the two axes (MondoA-Rubicon and MondoA-TFEB) is not serial but parallel, we investigated the potential relation between MondoA and TFEB during the acute phase. The nuclear translocation of TFEB was not increased in the kidneys 2 days after IRI *MondoA*$^{F/F}$ mice compared with sham-operated kidneys (Supplemental Figure 10B). The lack of increased nuclear translocation of TFEB is consistent with the fact that MondoA gene expression is also decreased in the kidneys of IRI *MondoA*$^{F/F}$ mice during the acute phase. In addition, the nuclear translocation of TFEB in *MondoA*-deficient IRI kidneys was not significantly different compared with that of *MondoA*$^{F/F}$ IRI kidneys, suggesting that MondoA-TFEB axis does not have a significant effect during the acute phase (Supplemental Figure 10, B and D). On the other hand, we examined the potential relation between and MondoA and Rubicon during the recovery phase after IRI. Rubicon expression was increased in *MondoA*-deficient IRI kidneys (Supplemental Figure 10C). These findings suggest that the two axes may be parallel. However, there is no increase in Rubicon expression in *Tfeb*-deficient IRI kidneys,

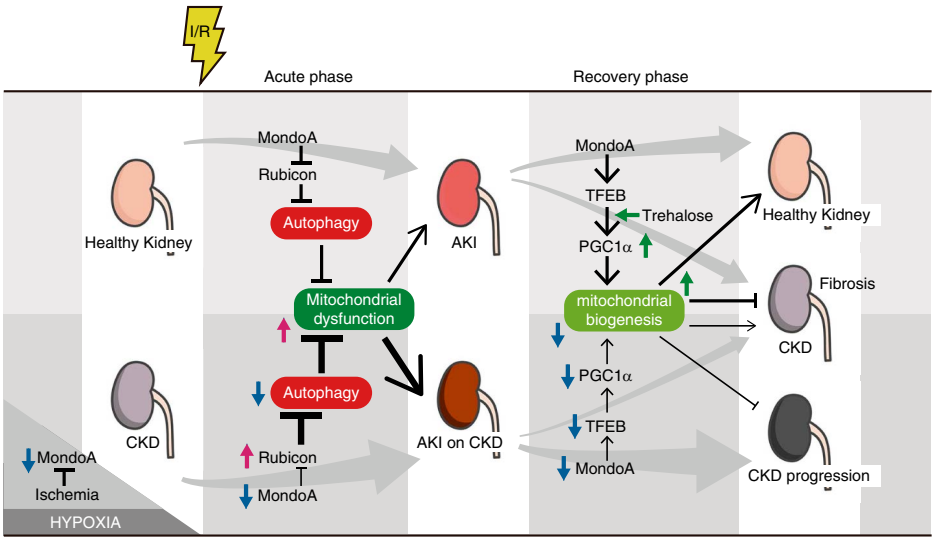

Figure 8. MondoA ameliorates AKI by increasing autophagic flux and prevents transition to CKD by promoting mitochondrial biogenesis. Schematic illustration of this study. The transcriptional activity of MondoA is suppressed in CKD patients and under hypoxic conditions. It is enhanced after reoxygenation: (*1*) MondoA activity induces autophagy because of decreased Rubicon and (*2*) MondoA reactivation counteracts the AKI-to-CKD transition through mitochondrial biogenesis *via* the TFEB-PGC1α axis. In elderly individuals or patients with CKD, the excessive expression of Rubicon because of decreased MondoA levels suppresses autophagy and exacerbates AKI on CKD after the acute phase of kidney injury. On the other hand, the reactivation of MondoA during the recovery phase of kidney injury leads the TFEB-PGC1α axis to sustain mitochondrial biogenesis. The use of a TFEB activator to target the MondoA-TFEB-PGC1α axis in elderly individuals or patients with CKD may hold promise in attenuating the progression to CKD during the recovery phase of kidney injury.

indicating that the MondoA-TFEB axis, independently of Rubicon, is protective against the AKI-to-CKD transition during the recovery phase (Supplemental Figure 10, C and D).

Of note, however, it is still unclear whether inducing MondoA overexpression during the acute and recovery phase of AKI is protective or not, because MondoA overexpression may increase the expression of Txnip, which is regulated by the other transcription factor, carbohydrate-response element-binding protein.[48,63] In particular, Txnip and carbohydrate-response element-binding protein are harmful in the context of diabetic kidney disease.[64,65] Thus, interventions targeting downstream factors, such as Rubicon inhibition and TFEB upregulation, can safely ameliorate these pathological conditions.

In conclusion, we report that MondoA plays a pivotal regulatory role in enhancing autophagy by suppressing Rubicon in the acute phase after AKI, while it promotes the TFEB-PGC1α pathway to sustain mitochondrial biogenesis during the recovery phase. These findings should pave the way for novel treatments for AKI and uncover strategies for protecting against the AKI-to-CKD transition.

Disclosures

Disclosure forms, as provided by each author, are available with the online version of the article at http://links.lww.com/JSN/E725.

Funding

T. Yoshimori: AMED (JP22gm1410014). T. Yamamoto: a Grant-in-Aid for Scientific Research from the Ministry of Education, Culture, Sports, Science, and Technology in Japan (21K08276), Takeda Science Foundation, Novartis Foundation, Novo Nordisk Pharma, and Manpei Suzuki Diabetes Foundation. S. Sakai: a Grant-in-Aid for Scientific Research from the Ministry of Education, Culture, Sports, Science, and Technology in Japan (22K16240). Y. Isaka: a Grant-in-Aid for Scientific Research from the Ministry of Education, Culture, Sports, Science, and Technology in Japan (21H02935).

Acknowledgments

We thank T. Matsusaka and F. Niimura, Tokai University School of Medicine for KAP-Cre mice; N. Mizushima, University of Tokyo, for GFP-MAP1LC3 mice and *Atg5*$^{F/F}$ mice; T. Michigami, Osaka Medical Center and Research Institute, for LRP2/MEGALIN antibody; and N. Horimoto for technical assistance.

Author Contributions

Conceptualization: Shihomi Maeda, Satoshi Minami, Shinsuke Sakai, Yoshitsugu Takabatake, Takeshi Yamamoto.
Data curation: Ryuya Edahiro, Atsuhiro Imai, Jun Matsuda, Isao Matsui, Tomoko Namba-Hamano, Yukinori Okada, Atsushi Takahashi.
Formal analysis: Ryuya Edahiro, Atsuhiro Imai, Sho Matsui, Jun Nakamura, Hiroaki Yonishi.
Funding acquisition: Yoshitaka Isaka, Shinsuke Sakai, Yoshitsugu Takabatake, Takeshi Yamamoto, Tamotsu Yoshimori.
Investigation: Shihomi Maeda, Shinsuke Sakai.
Methodology: Shihomi Maeda, Satoshi Minami, Shinsuke Sakai, Yoshitsugu Takabatake, Seiji Takashima, Hitomi Yamamoto-Imoto.
Project administration: Takeshi Yamamoto.
Resources: Andrea Ballabio, Ryoichi Imamura, Yoshitaka Isaka, Jun Matsuda, Isao Matsui, Satoshi Minami, Shuhei Nakamura, Tomoko Namba-Hamano, Norio Nonomura, Yukinori Okada, Shinsuke Sakai, Yoshitsugu Takabatake, Motoko Yanagita, Tamotsu Yoshimori.
Supervision: Yoshitaka Isaka.
Validation: Shihomi Maeda, Sho Matsui, Jun Nakamura, Shinsuke Sakai, Takeshi Yamamoto.
Visualization: Shihomi Maeda, Shinsuke Sakai.
Writing – original draft: Shihomi Maeda, Shinsuke Sakai.
Writing – review & editing: Andrea Ballabio, Yoshitaka Isaka, Satoshi Minami, Shuhei Nakamura, Yoshitsugu Takabatake, Takeshi Yamamoto, Motoko Yanagita, Tamotsu Yoshimori.

Data Sharing Statement

Previously published data were used for this study. *Nat Commun*. July 11, 2022; 13(1):4018. doi:10.1038/s41467-022-31772-9 (GSE180420). All data are available from the authors upon request.

Supplemental Material

This article contains the following supplemental material online at http://links.lww.com/JSN/E724.

Supplemental Table 1. Demographic and clinical features of patients whose kidney sections were immunostained.

Supplemental Table 2. Characteristics of patients whose kidney sections were immunostained.

Supplemental Table 3. Demographic and clinical features of kidney transplant donor whose kidney sections were immunostained.

Supplemental Figure 1. Analysis of human kidney biopsy samples.

Supplemental Figure 2. Transcriptional activity of MondoA in proximal tubular epithelial cells after IRI.

Supplemental Figure 3. Loss of *MondoA* impairs autophagy initiation and autophagosome maturation in cultured proximal tubular epithelial cells.

Supplemental Figure 4. Loss of *MondoA* exacerbates IRI.

Supplemental Figure 5. Levels of Prdx3 in proximal tubular epithelial cells are unchanged regardless of MondoA expression.

Supplemental Figure 6. Knockdown of *MondoA* in *Rubicon*-deficient proximal tubular epithelial cells.

Supplemental Figure 7. Alterations of mTORC1 and TFEB pathways in *MondoA*-deficient proximal tubular epithelial cells.

Supplemental Figure 8. Trehalose activates the TFEB pathway and ameliorates IRI in *MondoA*-deficient kidneys.

Supplemental Figure 9. ZLN005 activates PGC1α and ameliorates IRI in *MondoA*-deficient kidneys.

Supplemental Figure 10. The MondoA-TFEB axis during the acute phase and the MondoA–Rubicon axis during the recovery phase of IRI.

References

1. Chertow GM, Burdick E, Honour M, Bonventre JV, Bates DW. Acute kidney injury, mortality, length of stay, and costs in hospitalized patients. *J Am Soc Nephrol*. 2005;16(11):3365–3370. doi:10.1681/ASN.2004090740
2. Bihorac A, Yavas S, Subbiah S, et al. Long-term risk of mortality and acute kidney injury during hospitalization after major surgery. *Ann Surg*. 2009;249(5):851–858. doi:10.1097/SLA.0b013e3181a40a0b
3. Ishani A, Xue JL, Himmelfarb J, et al. Acute kidney injury increases risk of ESRD among elderly. *J Am Soc Nephrol*. 2009;20(1):223–228. doi:10.1681/ASN.2007080837
4. Lo LJ, Go AS, Chertow GM, et al. Dialysis-requiring acute renal failure increases the risk of progressive chronic kidney disease. *Kidney Int*. 2009;76(8):893–899. doi:10.1038/ki.2009.289
5. Chawla LS, Eggers PW, Star RA, Kimmel PL. Acute kidney injury and chronic kidney disease as interconnected syndromes. *N Engl J Med*. 2014;371(1):58–66. doi:10.1056/NEJMra1214243

6. He L, Wei Q, Liu J, et al. AKI on CKD: heightened injury, suppressed repair, and the underlying mechanisms. *Kidney Int.* 2017;92(5):1071–1083. doi:10.1016/j.kint.2017.06.030
7. Kimura T, Takabatake Y, Takahashi A, et al. Autophagy protects the proximal tubule from degeneration and acute ischemic injury. *J Am Soc Nephrol.* 2011;22(5):902–913. doi:10.1681/ASN.2010070705
8. Takahashi A, Kimura T, Takabatake Y, et al. Autophagy guards against cisplatin-induced acute kidney injury. *Am J Pathol.* 2012;180(2):517–525. doi:10.1016/j.ajpath.2011.11.001
9. Maejima I, Takahashi A, Omori H, et al. Autophagy sequesters damaged lysosomes to control lysosomal biogenesis and kidney injury. *EMBO J.* 2013;32(17):2336–2347. doi:10.1038/emboj.2013.171
10. Yamamoto T, Takabatake Y, Kimura T, et al. Time-dependent dysregulation of autophagy: implications in aging and mitochondrial homeostasis in the kidney proximal tubule. *Autophagy.* 2016;12(5):801–813. doi:10.1080/15548627.2016.1159376
11. Yamamoto T, Takabatake Y, Takahashi A, et al. High-Fat diet-induced lysosomal dysfunction and impaired autophagic flux contribute to lipotoxicity in the kidney. *J Am Soc Nephrol.* 2017;28(5):1534–1551. doi:10.1681/ASN.2016070731
12. Takahashi A, Takabatake Y, Kimura T, et al. Autophagy inhibits the accumulation of advanced glycation end products by promoting lysosomal biogenesis and function in the kidney proximal tubules. *Diabetes.* 2017;66(5):1359–1372. doi:10.2337/db16-0397
13. Sakai S, Yamamoto T, Takabatake Y, et al. Proximal tubule autophagy differs in type 1 and 2 diabetes. *J Am Soc Nephrol.* 2019;30(6):929–945. doi:10.1681/ASN.2018100983
14. Minami S, Sakai S, Yamamoto T, et al. FGF21 and autophagy coordinately counteract kidney disease progression during aging and obesity. *Autophagy.* 2024;20(3):489–504. doi:10.1080/15548627.2023.2259282
15. Yamamoto-Imoto H, Minami S, Shioda T, et al. Age-associated decline of MondoA drives cellular senescence through impaired autophagy and mitochondrial homeostasis. *Cell Rep.* 2022;38(9):110444. doi:10.1016/j.celrep.2022.110444
16. Matsunaga K, Saitoh T, Tabata K, et al. Two Beclin 1-binding proteins, Atg14L and Rubicon, reciprocally regulate autophagy at different stages. *Nat Cell Biol.* 2009;11(4):385–396. doi:10.1038/ncb1846
17. Stoltzman CA, Peterson CW, Breen KevinT, Muoio DM, Billin AN, Ayer DE. Glucose sensing by MondoA:Mlx complexes: a role for hexokinases and direct regulation of thioredoxin-interacting protein expression. *Proc Natl Acad Sci U S A.* 2008;105(19):6912–6917. doi:10.1073/pnas.0712199105
18. Peterson CW, Stoltzman CA, Sighinolfi MP, Han KS, Ayer DE. Glucose controls nuclear accumulation, promoter binding, and transcriptional activity of the MondoA-Mlx heterodimer. *Mol Cell Biol.* 2010;30(12):2887–2895. doi:10.1128/MCB.01613-09
19. Nakamura S, Karalay O, Jager PS, et al. Mondo complexes regulate TFEB via TOR inhibition to promote longevity in response to gonadal signals. *Nat Commun.* 2016;7:10944. doi:10.1038/ncomms10944
20. Kaadige MR, Yang J, Wilde BR, Ayer DE. MondoA-Mlx transcriptional activity is limited by mTOR-MondoA interaction. *Mol Cell Biol.* 2015;35(1):101–110. doi:10.1128/MCB.00636-14
21. Matsuda J, Takahashi A, Takabatake Y, et al. Metabolic effects of RUBCN/Rubicon deficiency in kidney proximal tubular epithelial cells. *Autophagy.* 2020;16(10):1889–1904. doi:10.1080/15548627.2020.1712107
22. Sergin I, Evans TD, Zhang X, et al. Exploiting macrophage autophagy-lysosomal biogenesis as a therapy for atherosclerosis. *Nat Commun.* 2017;8:15750. doi:10.1038/ncomms15750
23. Matsuda J, Maier M, Aoudjit L, Baldwin C, Takano T. ARHGEF7 (β-PIX) is required for the maintenance of podocyte architecture and glomerular function. *J Am Soc Nephrol.* 2020;31(5):996–1008. doi:10.1681/ASN.2019090982
24. Balzer MS, Doke T, Yang YW, et al. Single-cell analysis highlights differences in druggable pathways underlying adaptive or fibrotic kidney regeneration. *Nat Commun.* 2022;13(1):4018. doi:10.1038/s41467-022-31772-9
25. Nakamura J, Yamamoto T, Takabatake Y, et al. TFEB-mediated lysosomal exocytosis alleviates high-fat diet-induced lipotoxicity in the kidney. *JCI Insight.* 2023;8(4):e162498. doi:10.1172/jci.insight.162498
26. Endo T, Nakamura J, Sato Y, et al. Exploring the origin and limitations of kidney regeneration. *J Pathol.* 2015;236(2):251–263. doi:10.1002/path.4514
27. Yamamoto T, Takabatake Y, Minami S, et al. Eicosapentaenoic acid attenuates renal lipotoxicity by restoring autophagic flux. *Autophagy.* 2021;17(7):1700–1713. doi:10.1080/15548627.2020.1782034
28. Minami S, Yamamoto T, Takabatake Y, et al. Lipophagy maintains energy homeostasis in the kidney proximal tubule during prolonged starvation. *Autophagy.* 2017;13(10):1629–1647. doi:10.1080/15548627.2017.1341464
29. Namba T, Takabatake Y, Kimura T, et al. Autophagic clearance of mitochondria in the kidney copes with metabolic acidosis. *J Am Soc Nephrol.* 2014;25(10):2254–2266. doi:10.1681/ASN.2013090986
30. Fujimura R, Yamamoto T, Takabatake Y, et al. Autophagy protects kidney from phosphate-induced mitochondrial injury. *Biochem Biophys Res Commun.* 2020;524(3):636–642. doi:10.1016/j.bbrc.2020.01.137
31. Yamamuro T, Nakamura S, Yamano Y, et al. Rubicon prevents autophagic degradation of GATA4 to promote Sertoli cell function. *PLoS Genet.* 2021;17(8):e1009688. doi:10.1371/journal.pgen.1009688
32. Napolitano G, Di Malta C, Esposito A, et al. A substrate-specific mTORC1 pathway underlies Birt-Hogg-Dube syndrome. *Nature.* 2020;585(7826):597–602. doi:10.1038/s41586-020-2444-0
33. Kim J, Park K, Kim MJ, et al. An autophagy enhancer ameliorates diabetes of human IAPP-transgenic mice through clearance of amyloidogenic oligomer. *Nat Commun.* 2021;12(1):183. doi:10.1038/s41467-020-20454-z
34. Matsui I, Ito T, Kurihara H, Imai E, Ogihara T, Hori M. Snail, a transcriptional regulator, represses nephrin expression in glomerular epithelial cells of nephrotic rats. *Lab Invest.* 2007;87(3):273–283. doi:10.1038/labinvest.3700518
35. Mori D, Matsui I, Shimomura A, et al. Protein carbamylation exacerbates vascular calcification. *Kidney Int.* 2018;94(1):72–90. doi:10.1016/j.kint.2018.01.033
36. Rule AD, Amer H, Cornell LD, et al. The association between age and nephrosclerosis on renal biopsy among healthy adults. *Ann Intern Med.* 2010;152(9):561–567. doi:10.7326/0003-4819-152-9-201005040-00006
37. Sturmlechner I, Durik M, Sieben CJ, Baker DJ, van Deursen JM. Cellular senescence in renal ageing and disease. *Nat Rev Nephrol.* 2017;13(2):77–89. doi:10.1038/nrneph.2016.183
38. Kirita Y, Wu H, Uchimura K, Wilson PC, Humphreys BD. Cell profiling of mouse acute kidney injury reveals conserved cellular responses to injury. *Proc Natl Acad Sci U S A.* 2020;117(27):15874–15883. doi:10.1073/pnas.2005477117
39. Settembre C, De Cegli R, Mansueto G, et al. TFEB controls cellular lipid metabolism through a starvation-induced autoregulatory loop. *Nat Cell Biol.* 2013;15(6):647–658. doi:10.1038/ncb2718
40. Palmieri M, Impey S, Kang H, et al. Characterization of the CLEAR network reveals an integrated control of cellular clearance pathways. *Hum Mol Genet.* 2011;20(19):3852–3866. doi:10.1093/hmg/ddr306
41. Sardiello M, Palmieri M, di Ronza A, et al. A gene network regulating lysosomal biogenesis and function. *Science.* 2009;325(5939):473–477. doi:10.1126/science.1174447
42. Wang Z, Fu Z, Wang C, et al. ZLN005 protects against ischemia-reperfusion-induced kidney injury by mitigating oxidative stress through the restoration of mitochondrial fatty acid oxidation. *Am J Transl Res.* 2021;13(9):10014–10037. PMID: 34650679
43. Zhu P, Ma H, Cui S, et al. ZLN005 alleviates in vivo and in vitro renal fibrosis via PGC-1α-mediated mitochondrial homeostasis. *Pharmaceuticals (Basel).* 2022;15(4):434. doi:10.3390/ph15040434
44. Nangaku M. Chronic hypoxia and tubulointerstitial injury: a final common pathway to end-stage renal failure. *J Am Soc Nephrol.* 2006;17(1):17–25. doi:10.1681/ASN.2005070757
45. Tanaka S, Tanaka T, Nangaku M. Hypoxia as a key player in the AKI-to-CKD transition. *Am J Physiol Renal Physiol.*

2014;307(11):F1187–F1195. doi:10.1152/ajprenal.00425.2014
46. Chen PS, Chiu WT, Hsu PL, et al. Pathophysiological implications of hypoxia in human diseases. *J Biomed Sci.* 2020;27(1):63. doi:10.1186/s12929-020-00658-7
47. Kaadige MR, Looper RE, Kamalanaadhan S, Ayer DE. Glutamine-dependent anapleurosis dictates glucose uptake and cell growth by regulating MondoA transcriptional activity. *Proc Natl Acad Sci U S A.* 2009;106(35):14878–14883. doi:10.1073/pnas.0901221106
48. Richards P, Rachdi L, Oshima M, et al. MondoA is an essential glucose-responsive transcription factor in human pancreatic β-cells. *Diabetes.* 2018;67(3):461–472. doi:10.2337/db17-0595
49. Nah J, Zhai P, Huang CY, et al. Upregulation of Rubicon promotes autosis during myocardial ischemia/reperfusion injury. *J Clin Invest.* 2020;130(6):2978–2991. doi:10.1172/JCI132366
50. Nakamura S, Oba M, Suzuki M, et al. Suppression of autophagic activity by Rubicon is a signature of aging. *Nat Commun.* 2019;10(1):847. doi:10.1038/s41467-019-08729-6
51. Tanaka S, Hikita H, Tatsumi T, et al. Rubicon inhibits autophagy and accelerates hepatocyte apoptosis and lipid accumulation in nonalcoholic fatty liver disease in mice. *Hepatology.* 2016;64(6):1994–2014. doi:10.1002/hep.28820
52. Li Y, Pan Y, Cao S, et al. Podocyte EGFR inhibits autophagy through upregulation of Rubicon in type 2 diabetic nephropathy. *Diabetes.* 2021;70(2):562–576. doi:10.2337/db20-0660
53. Li L, Kang H, Zhang Q, D'Agati VD, Al-Awqati Q, Lin F. FoxO3 activation in hypoxic tubules prevents chronic kidney disease. *J Clin Invest.* 2019;129(6):2374–2389. doi:10.1172/JCI122256
54. Shi M, Flores B, Gillings N, et al. αKlotho mitigates progression of AKI to CKD through activation of autophagy. *J Am Soc Nephrol.* 2016;27(8):2331–2345. doi:10.1681/ASN.2015060613
55. Livingston MJ, Shu S, Fan Y, et al. Tubular cells produce FGF2 via autophagy after acute kidney injury leading to fibroblast activation and renal fibrosis. *Autophagy.* 2023;19(1):256–277. doi:10.1080/15548627.2022.2072054
56. Guillaume CCRB, Kishi S, Taguchi K, et al. Cyclin G1 and TASCC regulate kidney epithelial cell G2-M arrest and fibrotic maladaptive repair. *Sci Transl Med.* 2019;11(476):eaav4754. doi:10.1126/scitranslmed.aav4754
57. Tran MT, Zsengeller ZK, Berg AH, et al. PGC1α drives NAD biosynthesis linking oxidative metabolism to renal protection. *Nature.* 2016;531(7595):528–532. doi:10.1038/nature17184
58. Tran M, Tam D, Bardia A, et al. PGC-1α promotes recovery after acute kidney injury during systemic inflammation in mice. *J Clin Invest.* 2011;121(10):4003–4014. doi:10.1172/JCI58662
59. Fontecha-Barriuso M, Martin-Sanchez D, Martinez-Moreno JM, et al. The role of PGC-1α and mitochondrial biogenesis in kidney diseases. *Biomolecules.* 2020;10(2):347. doi:10.3390/biom10020347
60. Lynch MR, Tran MT, Ralto KM, et al. TFEB-driven lysosomal biogenesis is pivotal for PGC1α-dependent renal stress resistance. *JCI Insight.* 2019;5(8):e126749. doi:10.1172/jci.insight.126749
61. Evans TD, Zhang X, Jeong SJ, et al. TFEB drives PGC-1α expression in adipocytes to protect against diet-induced metabolic dysfunction. *Sci Signal.* 2019;12(606):eaau2281. doi:10.1126/scisignal.aau2281
62. Wang Y, Gunewardena S, Li F, et al. An FGF15/19-TFEB regulatory loop controls hepatic cholesterol and bile acid homeostasis. *Nat Commun.* 2020;11(1):3612. doi:10.1038/s41467-020-17363-6
63. Ahn B. The function of MondoA and ChREBP nutrient-sensing factors in metabolic disease. *Int J Mol Sci.* 2023;24(10):8811. doi:10.3390/ijms24108811
64. Han Y, Xu X, Tang C, et al. Reactive oxygen species promote tubular injury in diabetic nephropathy: the role of the mitochondrial ros-txnip-nlrp3 biological axis. *Redox Biol.* 2018;16:32–46. doi:10.1016/j.redox.2018.02.013
65. Shah A, Xia L, Masson EA, et al. Thioredoxin-interacting protein deficiency protects against diabetic nephropathy. *J Am Soc Nephrol.* 2015;26(12):2963–2977. doi:10.1681/ASN.2014050528

AFFILIATIONS

[1]Department of Nephrology, Osaka University Graduate School of Medicine, Osaka, Japan
[2]Department of Statistical Genetics, Osaka University Graduate School of Medicine, Suita, Japan
[3]Department of Respiratory Medicine and Clinical Immunology, Osaka University Graduate School of Medicine, Suita, Japan
[4]Department of Genetics, Osaka University Graduate School of Medicine, Osaka, Japan
[5]Department of Medical Biochemistry, Osaka University Graduate School of Medicine, Osaka, Japan
[6]Department of Urology, Nagasaki University Graduate School of Biomedical Sciences, Nagasaki, Japan
[7]Department of Urology, Osaka University Graduate School of Medicine, Osaka, Japan
[8]Department of Nephrology, Kyoto University Graduate School of Medicine, Kyoto, Japan
[9]Institute for the Advanced Study of Human Biology, Kyoto University, Kyoto, Japan
[10]Department of Genome Informatics, Graduate School of Medicine, The University of Tokyo, Tokyo, Japan
[11]Laboratory for Systems Genetics, RIKEN Center for Integrative Medical Sciences, Yokohama, Japan
[12]Laboratory of Statistical Immunology, Immunology Frontier Research Center (WPI-IFReC), Osaka University, Suita, Japan
[13]Premium Research Institute for Human Metaverse Medicine (WPI-PRIMe), Osaka University, Suita, Japan
[14]Telethon Institute of Genetics and Medicine (TIGEM), Naples, Italy
[15]Medical Genetics Unit, Department of Medical and Translational Science, Federico II University, Naples, Italy
[16]Department of Molecular and Human Genetics, Baylor College of Medicine, Houston, Texas
[17]Jan and Dan Duncan Neurological Research Institute, Texas Children's Hospital, Houston, Texas
[18]Department of Biochemistry, Nara Medical University, Nara, Japan
[19]Laboratory of Intracellular Membrane Dynamics, Graduate School of Frontier Biosciences, Osaka University, Osaka, Japan
[20]Integrated Frontier Research for Medical Science Division, Institute for Open and Transdisciplinary Research Initiatives (OTRI), Osaka University, Osaka, Japan